

# Astrophysical Consequences of Black Holes in Asymptotically Safe Quantum Gravity: Shadows and Strong Gravitational Lensing

Somi Aktar,<sup>1,\*</sup> Niyaz Uddin Molla,<sup>2,†</sup> Farook Rahaman,<sup>1,‡</sup> and G. Mustafa<sup>3,§</sup>

<sup>1</sup>*Department of Mathematics, Jadavpur University, Kolkata 700032, West Bengal, India*

<sup>2</sup>*Department of Mathematics, Indian Institute of Engineering Science and Technology, Shibpur, Howrah-711 103, India*

<sup>3</sup>*Department of Physics, Zhejiang Normal University, Jinhua 321004, People's Republic of China*

We investigate the astrophysical consequences of black holes in asymptotically safe quantum gravity, characterized by the parameters  $S_0$ ,  $S_2$ ,  $m_0$ , and  $m_2$ , in addition to the black hole mass  $M$ . To evaluate the physical validity of the fundamental asymptotically safe theory of quantum gravity black hole solutions, we analyze their gravitational lensing properties in the strong field regime. Specifically, we examine the shadow cast by the asymptotically safe quantum gravity black hole and constrain its parameters using observational data from the M87\* and Sgr A\* supermassive black holes. Our analysis reveals that, within the  $1\sigma$  confidence level, a significant portion of the parameter space for asymptotically safe quantum gravity black holes is consistent with the Event Horizon Telescope (EHT) observations of M87\* and Sgr A\*. This suggests these black holes are plausible candidates for describing astrophysical black holes. As an additional observational test, we perform a detailed investigation of the strong gravitational lensing properties of these black holes. We explore the fundamental strong lensing observables in detail, including the angular positions and separations of the lensed images, the relative magnifications, the radius of the outermost Einstein ring, and the relativistic time delay between images. We compare the predictions of the asymptotically safe quantum gravity black hole for each observable with those of the classical Schwarzschild solution using realistic astrophysical data. Our findings provide a pathway for testing asymptotically safe quantum gravity at galactic and extragalactic scales, offering new insights into the observational properties of black hole solutions within this framework.

## I. INTRODUCTION

The study of black holes offers a unique opportunity to test the predictions of General Relativity (GR) under extreme conditions. In the high-curvature regions surrounding black holes [1, 2], GR predicts phenomena such as time dilation, gravitational redshift, and the warping of space, which have been observed and confirmed through astrophysical measurements. The Schwarzschild and Kerr solutions to Einstein's field equations describe the spacetime around non-rotating and rotating black holes and provide the framework for understanding black hole properties. Observing black holes is crucial in gravitational and cosmological physics, unveiling the enigmatic entities that profoundly shape spacetime. Recent developments in observational astrophysics, such as gravitational wave detection [3] from black hole mergers and direct imaging of black hole shadows [4, 5], have provided empirical support for GR in strong gravitational fields. These observations not only affirm the theoretical pre-

dictions of GR but also open new avenues for exploring potential extensions to GR, especially as researchers seek to reconcile it with quantum mechanics. Thus, black holes serve as natural laboratories, allowing scientists to probe the limits of GR and explore the fundamental nature of gravity. GR is perturbatively non-renormalizable, except for pure gravity without interactions involving scalar fields at the one-loop level [6, 7]. Consequently, GR is generally regarded as an effective field theory, posing significant challenges in developing an entirely consistent quantum theory of gravity. Nevertheless, gravity can be accurately described within a specific range of energy and length scales by imposing a suitable cutoff at high energy scales. However, beyond these limits, particularly near black hole singularities, the classical formulation of GR becomes inadequate, necessitating the development of a new physical theory.

In recent years, significant advancements have been made in the field of black hole physics. However, a deeper investigation into the fascinating and complex features of black holes, particularly the formation of relativistic images, is still required. Key phenomena, including gravitational lensing [8], black hole shadows [9], and quasinormal modes [10], play a crucial role in enhancing our understanding of general relativity, modified gravity theories, quantum gravity, and quantum mechanics. Despite these advances, observing such

\* [somiaktar9@gmail.com](mailto:somiaktar9@gmail.com)

† [niyazuddin182@gmail.com](mailto:niyazuddin182@gmail.com)

‡ [rahaman@associates.iucaa.in](mailto:rahaman@associates.iucaa.in)

§ [gmustafa3828@gmail.com](mailto:gmustafa3828@gmail.com)

features poses considerable challenges due to technical limitations and the need for precise theoretical modeling. Increasing attention has been directed toward understanding the impact of quantum gravity effects near singularities. Models such as M-theory, string theory, and loop quantum gravity are among the leading frameworks explored in this regard. A comprehensive formulation of quantum gravity was presented in [11], where a scale-dependent action was proposed, and an exact renormalization group equation was derived. This work marks a significant step forward in unraveling the intricate dynamics of quantum gravity in the vicinity of singularities. Even when considering GR as the low-energy limit of a more comprehensive theory known as supergravity [12], the issue of non-renormalizability remains unresolved. However, supergravity mitigates the ultraviolet (UV) divergences by reducing the number of divergent terms through its underlying supersymmetry. The quest for a consistent quantization of gravity encountered a deadlock until the advent of a non-perturbative approach to renormalization known as asymptotic safety [13, 14]. This framework posits the existence of a fixed point in the UV limit within the renormalization group flow [15, 16], allowing the gravitational coupling constant to approach this fixed point such that physical quantities become insulated from unphysical divergences. Consequently, the resulting theory is deemed asymptotically safe, implying that unphysical divergences are likely absent at high energies [17, 18]. Asymptotically safe gravity (ASG) broadens the applicability of effective field theory approaches, enabling the removal of the UV cutoff and providing a comprehensive description across all energy scales. Since ASG has profound implications at short distances (or high-energy scales) and black holes serve as natural laboratories for exploring gravity in its most extreme conditions, it is worthwhile to investigate light propagation and the gravitational deflection angle within the ASG framework. Such studies can enhance our understanding of quantum gravity from a phenomenological standpoint and provide valuable insights from an observational perspective. Furthermore, the bending of light around black holes is instrumental in shaping their shadows. Extensive research has been conducted on black hole solutions within the ASG framework [19–22].

Asymptotic safety, often referred to as non-perturbative renormalizability, is a concept in quantum field theory that seeks to establish a consistent and predictive quantum theory of gravity. A central aspect of this approach is the existence of a nontrivial fixed point in the renormalization group flow of the theory, which governs the behavior of coupling constants in

the ultraviolet (UV) regime and ensures that physical quantities remain free from divergences. Originally proposed by Steven Weinberg as a means to formulate a theory of quantum gravity, the notion of a nontrivial fixed point as a potential UV completion applies to other field theories, particularly those that are perturbatively nonrenormalizable. In this study, we investigate the astrophysical scenario of black holes within the framework of asymptotically safe gravity [13] alongside the quantum theory of gravity, where gravitational interactions converge toward an ultraviolet fixed point at trans-Planckian scales. Over the past three decades, this quantum field theoretical approach to gravity has emerged as a prominent contender for a consistent quantum theory of gravity, particularly in the context of the functional renormalization group (FRG) method, beginning with Reuter’s seminal paper [23]. For recent reviews on this topic, see references [24–26].

The study of black hole shadows and gravitational lensing further enhances our understanding of GR and its predictions around these extreme objects. The images of the supermassive black holes M87\* [5, 27] and Sgr A\* [28, 29] offer critical insights for testing gravitational effects in the strong field regime. A key characteristic of a black hole’s image is its shadow, formed by light rays captured by the outer event horizon. The shape and size of the shadow depend on several factors, including the parameters of the black hole, the paths followed by the light rays, and the observer’s location. When light rays approach a black hole, photons with low orbital angular momentum are trapped by the black hole, while those with higher angular momentum escape their gravitational pull. As a result, a distant observer perceives a dark region in the sky, known as the black hole’s shadow. This shadow, a silhouette of the event horizon outlined against the bright background of accreting material, is a direct observational indicator of the black hole’s presence and characteristics. The shadow’s shape and size depend on the black hole’s mass, spin, and curvature of the surrounding spacetime, offering a valuable opportunity to test the predictions of GR in the strong-field regime. For a detailed discussion of black hole shadows and their potential for testing GR, see [30–46].

Gravitational lensing has become an invaluable tool for probing fundamental properties of gravitational fields. It plays a crucial role in the study of the large-scale structure of the Universe, the behavior of massive stellar objects, and the search for dark matter candidates. In this work, we suggest that gravitational lensing can also be employed to distinguish between differ-

ent gravitational theories, particularly between asymptotically safe quantum gravity and general relativity. The deflection of light by black holes and galaxies and the phenomenon of strong gravitational lensing form a significant area of research. It can potentially reveal novel astrophysical effects, providing unique signatures for testing modified theories of gravity. Observables obtained from relativistic images in strong lensing scenarios could help distinguish between different black hole metrics through high-precision observations. Gravitational lensing, a phenomenon predicted by Einstein in 1915 [47], although he initially doubted it would ever be observed. This occurs when massive objects like black holes bend and magnify light from objects behind them due to their immense gravitational fields. In the black hole regime, gravitational lensing provides a unique way to study the properties of these enigmatic objects and their influence on spacetime [48–54]. When light from a distant source, such as a star or galaxy, passes close to a black hole, it can be bent into arcs or multiple images, depending on the alignment. This effect also allows us to observe a black hole's shadow as the intense gravity bends light around the black hole, casting a silhouette against the backdrop of surrounding radiation. This effect not only magnifies distant objects but also distorts and duplicates their images, revealing information about the black hole's mass and spin and the geometry of spacetime near the event horizon. Recent images from the Event Horizon Telescope (EHT), capturing the shadow of the supermassive black hole in the galaxy M87, have provided empirical evidence that aligns closely with GR's theoretical predictions, showcasing both the accuracy and limitations of the theory. These observations contribute to our understanding of the gravitational dynamics around black holes while presenting new challenges and opportunities for testing GR under conditions inaccessible in any other environment. There are three primary types of gravitational lensing, classified based on the alignment of the source, lens, and observer, as well as the resulting effects on the observed light, each offering unique insights into the nature of these extreme objects. On the other hand, weak gravitational lensing involves minor distortions in the shape of background objects when light passes through a less intense gravitational field near a black hole. Microlensing occurs when a black hole or other compact object momentarily magnifies the light of a background star without creating multiple images. Strong gravitational lensing is particularly significant in the study of black holes because it produces highly visible and distinct effects, such as multiple images, arcs, or Einstein rings, which can be directly observed and analyzed.

The clarity and magnitude of the distortions caused by strong lensing make it an exceptionally powerful tool for probing the fundamental nature of black holes and the behavior of light and matter in their extreme gravitational fields. The study of strong gravitational lensing around black holes has made substantial progress since Darwin's initial work on photon orbits [55], in the Schwarzschild black hole spacetime. Building on this foundation, Virbhadra and Ellis formalized the concept of relativistic images [49], focusing on the strong-field regime where light passing near a black hole's photon sphere can generate multiple, highly curved images. A significant breakthrough came with Bozza's development of the strong deflection limit (SDL) [56], which provided an accurate framework for calculating light deflection in the proximity of black holes. Further advancements were made by Frittelli, Killing, and Newman, who enhanced analytical methods for solving the lens equation [57], while Bozza extended the SDL approach. This approach has been utilized across various spacetimes, including rotating and charged black holes, such as Reissner-Nordström and Kerr black holes [58, 59]. The SDL has proven to be a versatile tool, applied to classical black hole spacetimes and to modified scenarios like braneworld black holes and those arising in modified gravity theories [60–66]. Ongoing research continues to investigate gravitational lensing in diverse black hole spacetimes, including those described by higher-curvature gravity theories [67–70], as well as modifications of the traditional Schwarzschild geometry [71–75]. Several researchers have extensively explored the physical observables associated with strong lensing effects across a variety of gravitational models and black hole solutions. These studies have analyzed various astrophysical implications by examining parameters such as the angular positions of images, separations between them, magnifications, Einstein ring characteristics, and time delays in the formation of relativistic images [65, 69, 70, 76–79]. The present study investigates the shadow and strong gravitational lensing characteristics of black holes in asymptotically safe quantum gravity, emphasizing unique geometric properties absent in other well-known black hole solutions. Notable examples include the Van der Waals black hole [80], Kerr black hole [81], Simpson-Visser black hole [82], acoustic charged black hole [79, 83], hairy Kerr black hole [40], Kerr-Taub-NUT-Quintessence black hole [84], Kerr-Taub-NUT spacetime [85], Bardeen black hole [86], Reissner-Nordström (RN) black hole [87], and black holes from the Horndeski theory of gravity [88], among others. Gravitational lensing effects induced by various black holes have been studied both numerically and an-

alytically in the strong-field limit [89–91]. Kumar et al. [65] analyzed the strong gravitational lensing effects of a hairy black hole in Horndeski theory of gravity. They discussed the astrophysical consequences of various supermassive black holes due to the presence of hair in this theory and compared the results with those for the standard Schwarzschild black hole in general relativity. Islam et al. [76] studied gravitational lensing by the rotating Simpson-Visser black hole in the strong-field limit. They analyzed the astrophysical implications using examples of supermassive black holes. They demonstrated that strong gravitational lensing effects can distinguish the rotating Simpson-Visser black hole from the Kerr black hole. In a subsequent study, Islam et al. [70] investigated the strong gravitational lensing effects of the Bardeen black hole within the framework of four-dimensional Einstein-Gauss-Bonnet (EGB) gravity. They explored the astrophysical consequences by examining supermassive black holes modeled with the 4D EGB Bardeen black hole and compared the results with those for the standard Schwarzschild and Bardeen black holes. Similarly, Kumar et al. [64] explored gravitational lensing in regular electrically charged (REC) black hole spacetimes, as well as REC no-horizon spacetimes, in the strong-field regime. Their analysis focused on the astrophysical implications for supermassive black holes modeled with regular spacetimes, comparing the results with those of the Schwarzschild black hole.

This paper aims to extend the analysis of black hole shadows and strong gravitational lensing by incorporating the spacetime geometry of black holes in asymptotically safe quantum gravity. We explore how this promising framework, rooted in the fundamental asymptotically safe quantum gravity theory, leads to potentially observable consequences for black hole spacetimes. In particular, we focus on key lensing observables, such as the black hole shadow, deflection angle, image magnifications, and time delays, and compare them with predictions from the classical lensing scenario around a black hole in a vacuum. By analyzing the interaction between the black hole's gravitational and quantum fields, we aim to constrain the black hole parameters through observational signatures. These results carry significant implications for understanding the environment surrounding black holes, testing GR and alternative gravity theories, and probing the fundamental properties of asymptotically safe quantum gravity through astrophysical observations.

The present paper is organized as follows: Section II provides a brief overview of the black hole solutions in asymptotically safe quantum gravity, with a focus on the non-rotating case. In Section III, we derive the expres-

sion for the black hole shadow in asymptotically safe quantum gravity and present the first set of constraints on the solution parameters based on comparisons with observational data from M87\* and Sgr A\*. Section IV explores the strong gravitational lensing properties of the asymptotically safe quantum gravity black hole, with a detailed investigation of the associated lensing observables. Specific predictions for these observables are made using realistic astrophysical data. Finally, the conclusions and implications of our findings are discussed in Section V.

In what follows, we use natural units with  $G = c = 1$ , and adopt a signature convention of  $\{-+++ \}$

## II. BLACK HOLE SOLUTIONS IN ASYMPTOTICALLY SAFE QUANTUM GRAVITY

Asymptotically Safe Gravity is a prominent and rigorous approach to Quantum Gravity, grounded in the Quantum Field Theory (QFT) framework and inspired by the Wilsonian concept of renormalization. Proposed by Weinberg in 1976, the asymptotic safety conjecture posits that gravity can become a non-perturbatively renormalizable quantum theory if the gravitational RG flow reaches an interacting fixed point in the UV regime. Asymptotically safe gravity [24, 92] is regarded as one of the most conservative and well-founded frameworks for addressing the quantum nature of gravity. It asserts that the high-energy behavior of the gravitational RG trajectory is controlled by a UV fixed point, where all relevant running couplings stabilize at finite, non-zero values. This notion of "asymptotic safety" extends the familiar concept of "asymptotic freedom", in which couplings tend toward zero at high energies. While asymptotic freedom ensures that couplings vanish in the UV limit, asymptotic safety generalizes the idea by allowing couplings to approach constant, finite values. Both asymptotic freedom and asymptotic safety ensure that a theory is renormalizable and remains well-defined across all energy scales, providing a consistent UV-complete framework at either a free or interacting fixed point. Asymptotic safety introduces a specific scale dependence for the gravitational coupling in the ultraviolet (UV) regime, which is expected to address the curvature singularities present in classical theories. The concept of "quantum-improving" classical black hole spacetimes by elevating the Newtonian gravitational constant,  $G_N$ , to a scale-dependent variable has garnered significant attention [93–98]. This approach

aims to capture leading-order quantum effects, yielding several intriguing implications that merit further investigation. Recent reviews have also explored these developments in detail [99, 100].

Black holes in asymptotically safe quantum gravity are described by solutions derived from the quantum effective action and the associated quantum equations of motion. These solutions are formulated using multi-graviton correlation functions within the asymptotically safe quantum gravity framework and have been recently explored numerically by Pawłowski and Tränkle [101]. The effective action is given by

$$\Gamma[g_{\mu\nu}] = \frac{1}{16\pi} \int_x d^4x \sqrt{g} \left[ R(\Delta, R) + R f_{R^2}(\Delta) R + R_{\mu\nu} f_{R_{\mu\nu}^2}(\Delta) R^{\mu\nu} \right]. \quad (1)$$

Here, the functions  $f_{R^2}(\Delta)$  and  $f_{R_{\mu\nu}^2}(\Delta)$  correspond to two-point correlation functions of the curvature scalar and Ricci tensor, respectively. These functions, often referred to as form factors, capture generalized dispersion effects. Studies of such form factors have been presented in works such as [102] and [103–106]. For a comprehensive review of recent developments, see [107]. To derive black hole solutions within the framework of modified asymptotically safe gravity in quantum theory, one must solve the field equations obtained from the effective action  $\Gamma[\bar{g}]$  given by Eq. (1) [101].

The static, spherically symmetric metric in asymptotically safe quantum gravity can be expressed as [101]:

$$ds^2 = -f(r)dt^2 + g(r)^{-1}dr^2 + r^2(d\theta^2 + \sin^2\theta d\phi^2), \quad (2)$$

where the metric function can be expressed as:

$$f(r) = 1 - \frac{2M}{r} + S_0 \frac{e^{-m_0 r}}{r} + S_2 \frac{e^{-m_2 r}}{r}, \quad (3)$$

$$g(r) = 1 - \frac{2M}{r} - S_0 \frac{e^{-m_0 r}}{r} (1 + m_0 r) + \frac{1}{2} S_2 \frac{e^{-m_2 r}}{r} (1 + m_2 r). \quad (4)$$

The two free parameters,  $S_0$  and  $S_2$ , govern the strength of the exponentially decaying Yukawa corrections. The masses  $m_0$  and  $m_2$  correspond to the spin-0 and spin-2 modes, respectively, and are linked to the couplings of various curvature terms. For the initial conditions  $(S_0, S_2) = (0, 0)$ , the asymptotically safe quantum gravity black hole metric (2) reduces to the classical Schwarzschild metric. The event horizon, located at  $r_h$ , is determined by the solution to the equation  $g(r_h) = 0$ .

### III. SHADOW OF A BLACK HOLE IN ASYMPTOTICALLY SAFE QUANTUM GRAVITY

In this section, we initiate our investigation of the black hole shadow within the asymptotically safe quantum gravity framework, focusing on the motion of photons and the resulting shadow. Our analysis begins by examining the trajectories of light in the spacetime of an asymptotically safe quantum gravity black hole. Furthermore, we aim to constrain the black hole parameters associated with this asymptotically safe quantum gravity quantum gravity model. Now using Eq. (3) we can introduce the function  $\gamma(r)$  (it was recently introduced in Refs. [108–110]):

$$\gamma^2(r) = \frac{r^2}{f(r)}. \quad (5)$$

The radius of a circular light orbit, particularly the one defining the photon sphere with radius  $r_{ph}$ , is found by solving the following condition [108]:

$$\left. \frac{d(\gamma^2(r))}{dr} \right|_{r=r_{ph}} = 0. \quad (6)$$

The photon orbit radii  $r_{ph}$  in asymptotically safe quantum gravity can be determined numerically using this equation.

When the parameters  $S_0 = S_2 = 0$ , the solution yields  $r_{ph} = 3M$  [108, 110], corresponding to the photon orbit radius in the Schwarzschild spacetime. We now analyze the shadow of the black hole within the asymptotically safe quantum gravity framework.

The angular radius of the black hole shadow is given by the following relation [108]:

$$\sin^2 \alpha_{sh} = \frac{\gamma^2(r_{ph})}{\gamma^2(r_{obs})}, \quad (7)$$

where  $\alpha_{sh}$  denotes the angular radius of the black hole shadow, and  $r_{obs}$  is the observer's distance, assumed to be very large but finite. For instance, the observer distance for Sgr A\* is  $r_{obs} = D \simeq 8.3$  kpc [28], while for M87\*, it is  $r_{obs} = D \simeq 16.8$  Mpc [5].

The quantity  $r_{ph}$  represents the radius of the photon sphere, as mentioned earlier. By combining Eqs. (5) and (6), it follows that for a distant observer, Eq. (7) can be rewritten as [108, 111]:

$$\sin^2 \alpha_{sh} = \frac{r_{ph}^2}{f(r_{ph})} \frac{f(r_{obs})}{r_{obs}^2}. \quad (8)$$

The radius of the black hole shadow for an observer at large distances can be determined using Eq. (8), yielding

the following expression [108, 111]:

$$R_{sh} \simeq r_{obs} \sin \alpha_{sh} \simeq \frac{r_{ph}}{\sqrt{f(r_{ph})}}. \quad (9)$$

This equation allows us to examine how the shadow radius of the black hole depends on the parameters of asymptotically safe quantum gravity.

The dependence of the black hole shadow on the parameters  $S_0$ ,  $S_2$ ,  $m_0$ , and  $m_2$  is illustrated in Fig. 1. It is evident that as the numerical values of the parameters  $S_0 > 0$  or  $S_2 > 0$  increase while keeping the other parameters fixed, the size of the black hole shadow decreases. Conversely, an increase in the values of the parameters  $m_0 > 0$  or  $m_2 > 0$ , with the other parameters held constant, increases the size of the black hole shadow.

#### A. Constraints the black hole parameters with the observational data from M87\* and Sgr A\*

Now, we aim to determine the possible ranges of the free parameters of the black hole in asymptotically safe quantum gravity by utilizing observational data from the supermassive black holes M87\* and Sgr A\*. Specifically, we will explore the theoretical constraints on the black hole parameters  $S_0$ ,  $S_2$ ,  $m_0$ , and  $m_2$  pairwise while keeping the remaining two parameters fixed.

To achieve this, we use the shadow data provided by the Event Horizon Telescope (EHT) project. The objective is to constrain the parameter pairs  $(S_0, S_2)$  and  $(m_0, m_2)$  by fitting them against the observed shadow sizes of M87\* and Sgr A\* within the framework of asymptotically safe quantum gravity. This approach will allow us to impose meaningful constraints on these parameters using real observational data.

The angular diameter of the shadow, the distance from the Sun to the black hole, and the mass of the black hole at the center of the galaxy M87 are given as  $\Omega_{M87^*} = 42 \pm 3 \mu\text{as}$ ,  $D = 16.8 \pm 0.8 \text{ Mpc}$ , and  $M_{M87^*} = (6.5 \pm 0.7) \times 10^9 M_\odot$ , respectively [112].

For Sgr A\*, the most recent data obtained by the EHT project are  $\Omega_{\text{Sgr A}^*} = 51.8 \pm 2.3 \mu\text{as}$ ,  $D = 8277 \pm 9 \pm 33 \text{ pc}$ , and  $M_{\text{Sgr A}^*} = 4.297 \pm 0.013 \times 10^6 M_\odot$  (from VLTI observations) [28].

Using these observational data, we can estimate the diameter of the shadow cast by the black hole per unit mass, using the following expression [111, 113, 114]:

$$d_{sh} = \frac{D \Omega}{M}. \quad (10)$$

Now we can obtain the diameter of the shadow from the expression  $d_{sh}^{\text{theo}} = 2R_{sh}$ . Thus, the diameter of the

BH shadow image is  $d_{sh}^{\text{M87}^*} = (11 \pm 1.5)M$  for M87\* and  $d_{sh}^{\text{Sgr A}^*} = (9.5 \pm 1.4)M$  for Sgr A\*. The angular diameters of the shadows of the black hole in asymptotically safe quantum gravity, obtained using the M87\* and Sgr A\* data, are depicted in Fig. 2, respectively.

#### CONSTRAINTS FROM M87\*

The shadow's angular diameter ( $\Omega$ ) for the M87\* black hole, averaged within the range of 32 to 45  $\mu\text{as}$  with a  $1\sigma$  region from EHT observations, imposes constraints on the parameter pairs  $(S_0, S_2)$  and  $(m_0, m_2)$  of the black hole in asymptotically safe quantum gravity, as shown in Figs. 2(a) and 2(c).

Here, the shadow's angular diameter ( $\Omega$ ) is expressed as a function of the parameter pairs  $(S_0, S_2)$  and  $(m_0, m_2)$ . In Fig. 2(a), the green and blue lines correspond to  $\Omega = 39.1 \mu\text{as}$  and  $\Omega = 39.5 \mu\text{as}$ , respectively. Similarly, in Fig. 2(c), the green and blue lines correspond to  $\Omega = 39.4 \mu\text{as}$  and  $\Omega = 39.3 \mu\text{as}$ , respectively. The blue and green curves in Figs. 2(a) and 2(c) align with the shadow size of M87\* observed by the EHT.

The constraints on the parameter pair  $(S_0, S_2)$  are given by (see Table I):  $0 \leq S_2/2M \leq 0.09$ , and  $0 \leq S_2/2M \leq 0.09$ , corresponding to  $\Omega = 39.1 \mu\text{as}$ . Similarly, the constraints on the parameter pair  $(m_0, m_2)$  are:  $0 \leq 2Mm_0 \leq 0.78$ , and  $0 \leq 2Mm_0 \leq 0.78$ , corresponding to  $\Omega = 39.4 \mu\text{as}$ .

Thus, M87\* can be modeled within this constrained parameter space as a black hole in asymptotically safe quantum gravity. The numerous possible parameter points within the parameter spaces  $(S_0, S_2)$  and  $(m_0, m_2)$  indicate that the compatibility of the black hole model in asymptotically safe quantum gravity with M87\* observations makes it a strong candidate for describing astrophysical black holes.

#### CONSTRAINTS FROM Sgr A\*

The shadow's angular diameter ( $\Omega$ ) for the Sgr A\* black hole, averaged within the range of 49.5 to 54.1  $\mu\text{as}$  with a  $1\sigma$  region from EHT observations, imposes constraints on the parameter pairs  $(S_0, S_2)$  and  $(m_0, m_2)$  of the black hole in asymptotically safe quantum gravity, as shown in Figs. 2(b) and 2(d).

Here, the shadow's angular diameter ( $\Omega$ ) is expressed as a function of the parameter pairs  $(S_0, S_2)$  and  $(m_0, m_2)$  (see in Fig. 2). In Fig. 2(b), the green and blue lines correspond to  $\Omega = 51.4 \mu\text{as}$  and  $\Omega = 51.8 \mu\text{as}$ , respectively. Similarly, in Fig. 2(d), the green and blue lines corre-

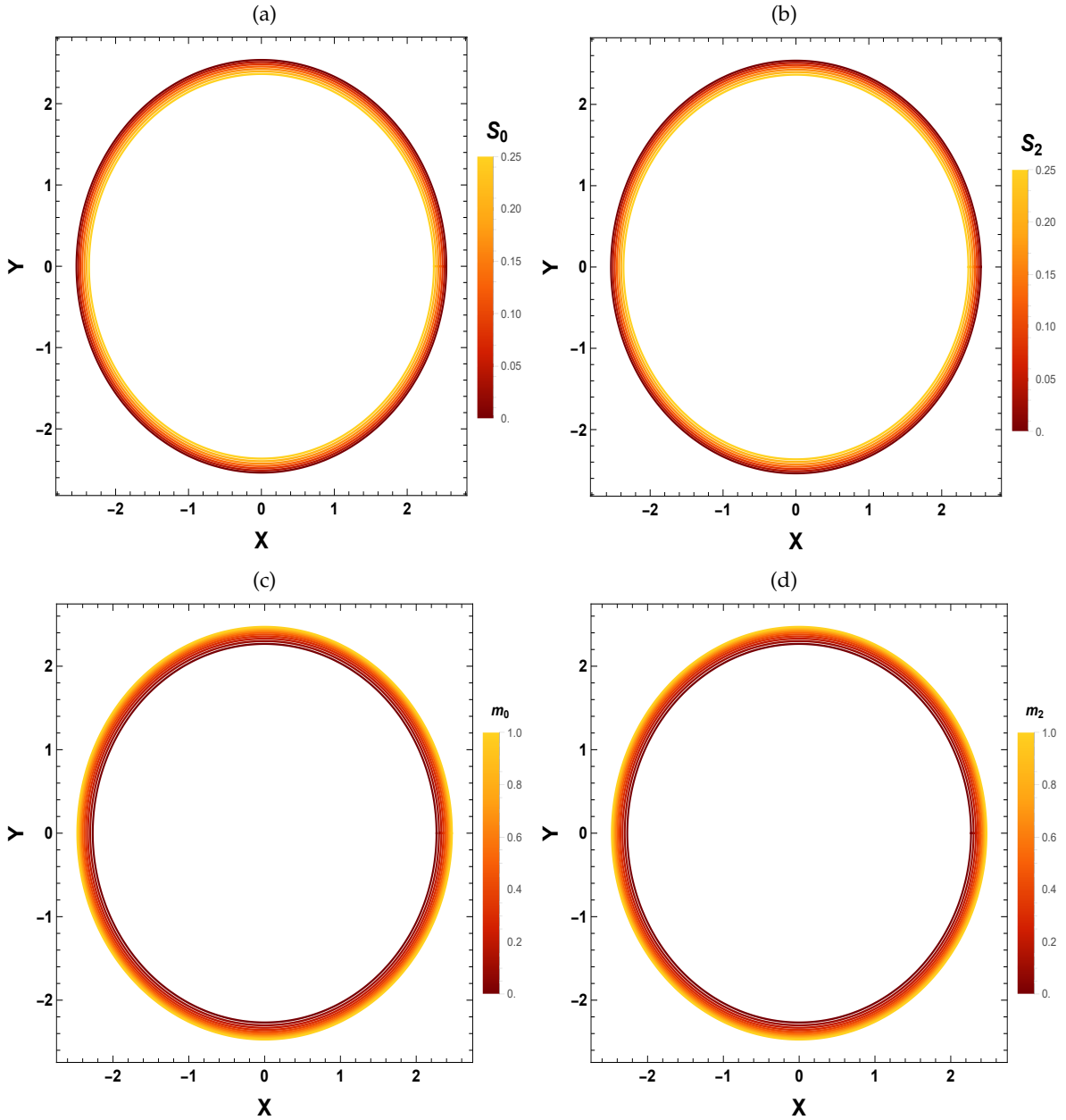


FIG. 1: The shadow silhouette of the black hole in asymptotically safe quantum gravity is presented in the X-Y plane ( $R_{sh} = \sqrt{X^2 + Y^2}$ ), with black hole parameters  $S_0, S_2, m_0$  and  $m_2$  varied independently, while the other parameters are kept fixed.

spond to  $\Omega = 52.2 \mu\text{as}$  and  $\Omega = 52 \mu\text{as}$ , respectively. The blue and green curves in Figs. 2(b) and 2(d) align with the shadow size of Sgr A\* observed by the EHT.

The constraints on the parameter pair  $(S_0, S_2)$  are given by (See Table I):  $0 \leq S_0/2M \leq 0.11$ , and  $0 \leq S_2/2M \leq 0.11$ , corresponding to  $\Omega = 51.4 \mu\text{as}$ . Similarly, the constraints on the parameter pair  $(m_0, m_2)$  are:  $0 \leq 2Mm_0 \leq 0.78$  and  $0 \leq 2Mm_2 \leq 0.78$ , corresponding to  $\Omega = 52.2 \mu\text{as}$ .

Thus, Sgr A\* can be modeled as a black hole in asymptotically safe quantum gravity within this constrained parameter space. The numerous possible parameter points within the parameter spaces  $(S_0, S_2)$  and  $(m_0, m_2)$  indicate that the compatibility of the black hole model in asymptotically safe quantum gravity with Sgr A\* observations makes it a strong candidate for describing astrophysical black holes.

Supermassive BH	$\Omega(\mu\text{as})$	$S_0/2M$	$S_2/2M$	$2Mm_0$	$2Mm_2$
M87*	39.1	$0 < S_0/2M \leq 0.09$	$0 < S_2/2M \leq 0.09$	1	1
	39.5	$0 < S_0/2M \leq 0.047$	$0 < S_2/2M \leq 0.047$	1	1
	39.3	0.01	0.01	$0 < 2Mm_0 \leq 0.39$	$0 < 2Mm_0 \leq 0.39$
	39.4	0.01	0.01	$0 < 2Mm_0 \leq 0.78$	$0 < 2Mm_0 \leq 0.78$
Sgr A*	51.4	$0 < S_0/2M \leq 0.11$	$0 < S_2/2M \leq 0.11$	1	1
	51.8	$0 < S_0/2M \leq 0.079$	$0 < S_2/2M \leq 0.079$	1	1
	52.2	0.01	0.01	$0 < 2Mm_0 \leq 1.8$	$0 < 2Mm_0 \leq 1.8$
	52	0.01	0.01	$0 < 2Mm_0 \leq 0.55$	$0 < 2Mm_0 \leq 0.55$

TABLE I: Estimated ranges of the asymptotically safe quantum gravity black hole parameters  $S_0$ ,  $S_2$  and  $m_0$ ,  $m_2$  from the known shadow observables  $\Omega(\mu\text{as})$  for M87\* and Sgr A\*.

#### IV. STRONG GRAVITATIONAL LENSING AND ITS OBSERVABLES

In this section, we examine the phenomenon of strong gravitational lensing in the vicinity of a black hole in asymptotically safe quantum gravity. Our goal is to understand how the black hole parameters  $S_0$ ,  $S_2$ ,  $m_0$ , and  $m_2$  influence the observable outcomes of strong lensing and to compare the lensing behavior of the asymptotically safe quantum gravity black hole with that of the Schwarzschild black hole ( $S_0 = 0 = S_2$ ).

We begin our analysis by considering the strong deflection angle of a light ray within the equatorial plane ( $\theta = \frac{\pi}{2}$ ) of the black hole.

##### A. The strong lensing angle

To obtain the strong deflection angle of a light ray in the equatorial plane ( $\theta = \frac{\pi}{2}$ ) of a black hole, we rewrite first the metric (2) by redefining the quantities  $r$ ,  $t$ ,  $S_0$ ,  $S_2$ ,  $m_0$  and  $m_2$  in units of the radius  $2M$ , so that  $t \rightarrow t/2M$ ,  $r \rightarrow r/2M$ ,  $S_0 \rightarrow S_0/2M$ ,  $S_2 \rightarrow S_2/2M$ ,  $m_0 \rightarrow 2Mm_0$  and  $m_2 \rightarrow 2Mm_2$ , respectively. Hence, the asymptotically safe quantum geometric metric (2) takes in the equatorial approximation the form

$$d\bar{s}^2 = -A(r)dt^2 + B(r)dr^2 + C(r)d\phi^2, \quad (11)$$

where the metric function can be expressed as:

$$A(r) = 1 - \frac{1}{r} + S_0 \frac{e^{-m_0 r}}{r} + S_2 \frac{e^{-m_2 r}}{r}, \quad (12)$$

$$B(r) = \frac{1}{1 - \frac{1}{r} - S_0 \frac{e^{-m_0 r}}{r} (1 + m_0 r) + \frac{1}{2} S_2 \frac{e^{-m_2 r}}{r} (1 + m_2 r)}. \quad (13)$$

and

$$C(r) = r^2, \quad (14)$$

respectively. Gravitational lensing in the strong-field regime is governed by the interplay between the deflection angle and the lens equation. The null geodesic equation is given by

$$\dot{r} = \frac{dr}{d\tau} = \pm \sqrt{\frac{1}{B(r)} \left( \frac{E^2}{A(r)} - \frac{L^2}{r^2} \right)}, \quad (15)$$

where the constants  $E$  and  $L$  represent the energy and angular momentum of the particle, respectively. The parameter  $\tau$  is the affine parameter along the geodesic, while the functions  $A(r)$  and  $B(r)$  are given by Eqs. (12) and (13).

The unstable circular photon orbit, with radius  $r_{ph}$ , can be obtained from the conditions on the effective potential, given by  $\frac{dV_{eff}}{dr} \Big|_{r_{ph}} = 0$  and  $\frac{d^2V_{eff}}{dr^2} \Big|_{r_{ph}} < 0$ , respectively. Thus, the radius of the photon sphere  $r_{ph}$  is the largest real root of the equation [115–117]:

$$2A(r_{ph}) - r_{ph}A'(r_{ph}) = 0. \quad (16)$$

When a particle approaches the black hole at the closest distance  $r = r_0$ , where  $\frac{dr}{d\tau} = 0$ , the minimum impact parameter  $u_0$  can be defined in terms of the closest distance  $r_0$  [56] as:

$$u_0 = \frac{r_0}{\sqrt{A(r_0)}}. \quad (17)$$

The critical impact parameter for the unstable photon orbit is expressed as:

$$u_{ph} = \frac{r_{ph}}{\sqrt{A(r_{ph})}}, \quad (18)$$

where  $r_{ph}$  is the radius of the photon sphere.

The behavior of the photon sphere radius,  $r_{ph}$ , and the critical impact parameter,  $u_{ph}$ , are expressed as functions of the parameter pairs  $(S_0, S_2)$  and  $(m_0, m_2)$  (see

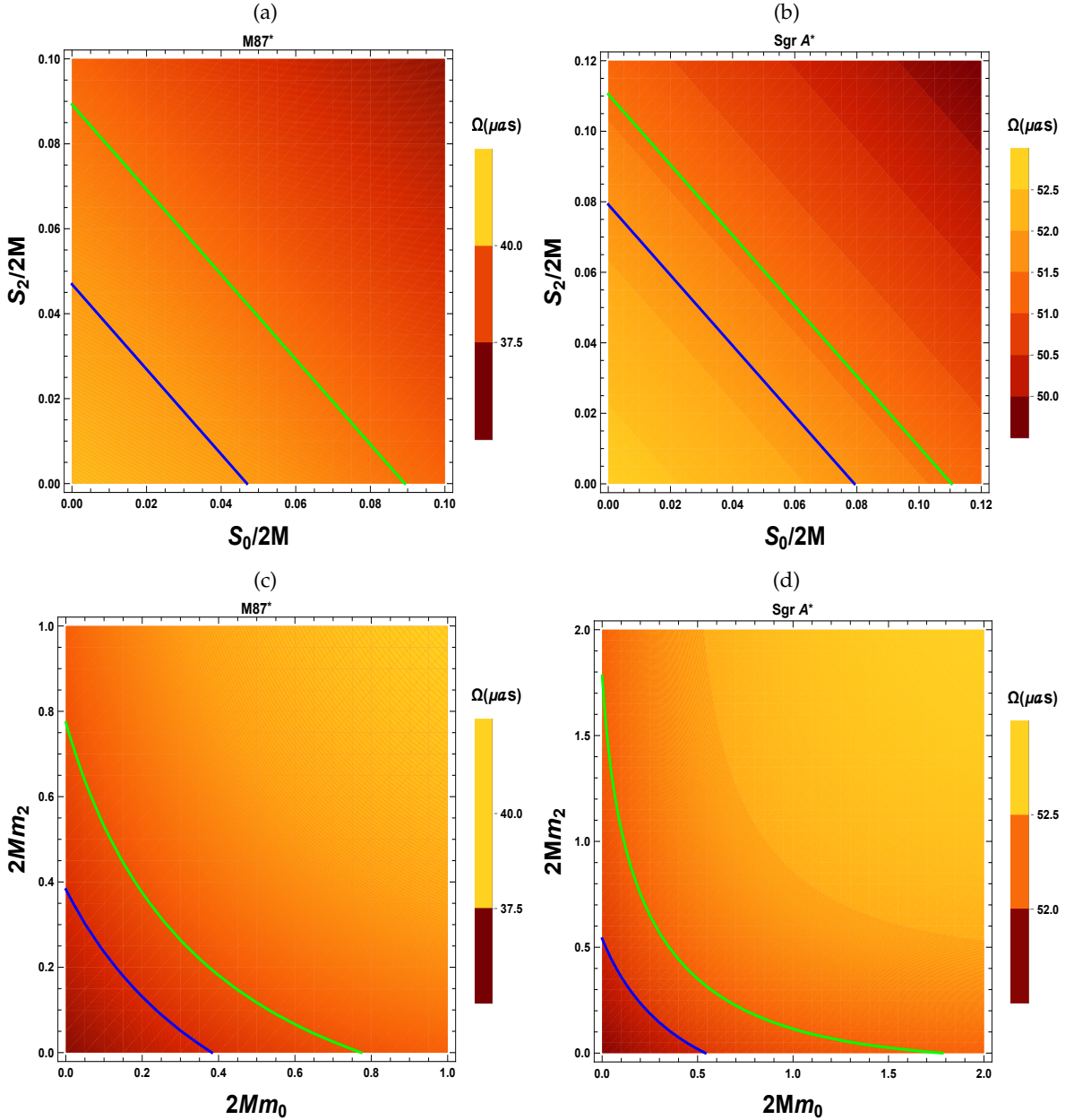


FIG. 2: The angular diameter  $\Omega(\mu\text{as})$  of the black hole shadow is presented as a function of the parameters  $S_0$ ,  $S_2$  and  $m_0$ ,  $m_2$  for the M87\* (panels (a) and (c)) and Sgr A\* (panels (b) and (d)) supermassive black holes. The enclosed regions satisfy the  $1-\sigma$  shadow bounds for M87\* and Sgr A\*, respectively. In panel (a), the green and blue lines correspond to  $\Omega = 39.1 \mu\text{as}$  and  $\Omega = 39.5 \mu\text{as}$ , respectively; in panel (b), they correspond to  $\Omega = 51.4 \mu\text{as}$  and  $\Omega = 51.8 \mu\text{as}$ , respectively; in panel (c), to  $\Omega = 39.4 \mu\text{as}$  and  $\Omega = 39.3 \mu\text{as}$ , respectively; and in panel (d), to  $\Omega = 52.2 \mu\text{as}$  and  $\Omega = 52 \mu\text{as}$ , respectively.

Figs. 3 and 4). It is observed from Fig. 3 that as the numerical values of the parameters  $S_0 > 0$  or  $S_2 > 0$  increase while keeping the other parameters fixed, the photon sphere radius  $r_{ph}$  decreases. Conversely, an increase in the values of the parameters  $m_0 > 0$  or  $m_2 > 0$ , with the other parameters held constant, increases

the photon sphere radius,  $r_{ph}$ . Furthermore, the photon sphere radius  $r_{ph}$  reaches its maximum ( $r_{ph} = 1.5$ ) when both  $S_0 \rightarrow 0$  and  $S_2 \rightarrow 0$ , corresponding to Schwarzschild black hole.

It is also observed from Fig. 4 that as the numerical values of the parameters  $S_0 > 0$  or  $S_2 > 0$  increase while

keeping the other parameters fixed, the critical impact parameter,  $u_{ph}$ , decreases. Conversely, an increase in the values of the parameters  $m_0 > 0$  or  $m_2 > 0$ , with the other parameters held constant, results in an increase in the critical impact parameter,  $u_{ph}$  (see Table II). Furthermore, the critical impact parameter  $u_{ph}$  reaches its maximum ( $u_{ph} = 2.59808$ ) when both  $S_0 \rightarrow 0$  and  $S_2 \rightarrow 0$ , corresponding to Schwarzschild black hole.

The strong deflection angle in the asymptotically safe quantum gravity black hole spacetime can be obtained

as a function of the closest approach distance  $r_0$  as [31]

$$\alpha_D(r_0) = I(r_0) - \pi = 2 \int_{r_0}^{\infty} \frac{\sqrt{B(r)} dr}{\sqrt{C(r)} \sqrt{\frac{A(r_0)C(r)}{A(r)C(r_0)} - 1}} - \pi. \quad (19)$$

The strong deflection angle  $\alpha_D(r_0)$  depends on the relationship between  $r_0$  and  $r_{ph}$ , and it increases when these two values are approximately equal (i.e.,  $r_0 \approx r_{ph}$ ). Hence, we introduce a new variable  $z$  defined as [118, 119]

$$z = 1 - \frac{r_0}{r}. \quad (20)$$

When  $r_0 \approx r_{ph}$ , the deflection angle takes on the following form [118, 120]

$$\alpha_D(u) = -\bar{a} \log \left( \frac{u}{u_{ph}} - 1 \right) + \bar{b} + \mathcal{O}((u - u_{ph}) \log(u - u_{ph})), \quad (21)$$

where

$$\begin{aligned} \bar{a} = & \left[ 4e^{(m_0+m_2)r_{ph}} \left( (r_{ph}-1)e^{(m_0+m_2)r_{ph}} + S_2 e^{m_0 r_{ph}} + S_0 e^{m_2 r_{ph}} \right) \right]^{\frac{1}{2}} \times \left[ \left( -2S_0 (m_0 r_{ph} + 1) e^{m_2 r_{ph}} + S_2 e^{m_0 r_{ph}} (m_2 r_{ph} + 1) \right) \right. \\ & \left. + 2(r_{ph}-1) e^{(m_0+m_2)r_{ph}} \right) \left( m_0 S_0 (m_0 r_{ph} + 2) (-e^{m_2 r_{ph}}) - m_2 S_2 e^{m_0 r_{ph}} (m_2 r_{ph} + 2) + 2e^{(m_0+m_2)r_{ph}} \right) \right]^{-\frac{1}{2}}, \end{aligned} \quad (22)$$

and

$$\bar{b} = b + I_R(r_{ph}), \quad (23)$$

where,

$$b = \bar{a} \times \log \left( -\frac{r_{ph} \left( m_0 S_0 (m_0 r_{ph} + 2) e^{m_2 r_{ph}} + m_2 S_2 e^{m_0 r_{ph}} (m_2 r_{ph} + 2) - 2e^{(m_0+m_2)r_{ph}} \right)}{(r_{ph}-1) e^{(m_0+m_2)r_{ph}} + S_2 e^{m_0 r_{ph}} + S_0 e^{m_2 r_{ph}}} \right), \quad (24)$$

and

$$I_R(r_{ph}) = 2 \int_0^1 r_{ph} \left( \left[ \sqrt{\frac{B(z)}{C(z)}} \left( \frac{A(r_{ph})}{C(r_{ph})} \frac{C(z)}{A(z)} - 1 \right)^{-\frac{1}{2}} \frac{1}{(1-z)^2} \right] - \frac{\bar{a}}{z r_{ph}} \right) dz, \quad (25)$$

where the integral must be evaluated numerically. We

numerically calculate the values of the critical impact

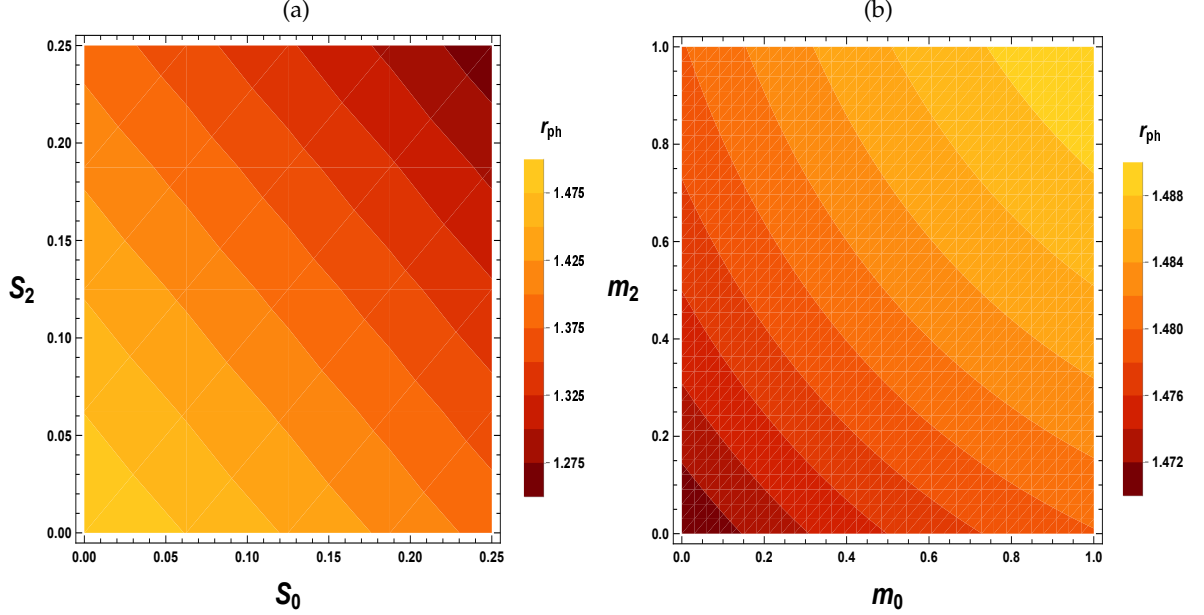


FIG. 3: The photon sphere radius  $r_{ph}$  is presented as a function of the parameters  $S_0$ ,  $S_2$  and  $m_0$ ,  $m_2$ .

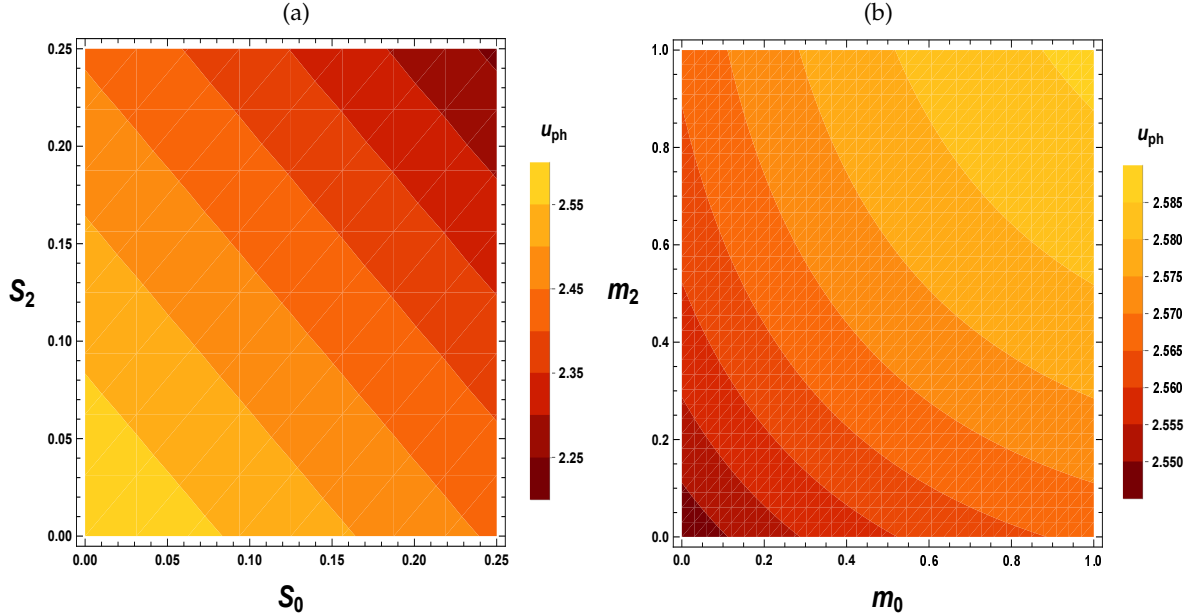


FIG. 4: The critical impact parameter  $u_{ph}$  is presented as a function of the parameters  $S_0$ ,  $S_2$  and  $m_0$ ,  $m_2$ .

parameter  $u_{ph}$  and of the strong lensing coefficients  $\bar{a}$  and  $\bar{b}$  at  $r = r_{ph}$  for the asymptotically safe quantum gravity black hole parameters  $S_0 = 0, 0.5, S_2 = 0, 0.1, 0.2, 0.3$ ,  $m_0 = 0.5, 1$ , and  $m_2 = 0.3, 0.6, 0.9, 1.1$ , respectively. The results are presented in Table II.

The behavior of the lensing coefficients  $\bar{a}$  and  $\bar{b}$  are expressed as functions of the parameter pairs  $(S_0, S_2)$  and  $(m_0, m_2)$  (see Figs. 5 and 6). It is observed from Fig. 3 that as the numerical values of the parameters  $S_0 > 0$

or  $S_2 > 0$  increase while keeping the other parameters fixed, the lensing coefficient  $\bar{a}$  increases. Similarly, an increase in the values of the parameters  $m_0 > 0$  or  $m_2 > 0$ , with the other parameters held constant, also results in a decrease in the value of the lensing coefficient  $\bar{a}$  (see Table II). The lensing coefficient  $\bar{a}$  reaches the minimum value  $\bar{a} = 1$  [56] when both  $S_0 \rightarrow 0$  and  $S_2 \rightarrow 0$ , corresponding to Schwarzschild black hole. Furthermore, Fig. 6 shows that as the numerical values of the param-

eters  $S_0 > 0$  or  $S_2 > 0$  increase, while keeping the other parameters fixed, the lensing coefficient  $\bar{b}$  first decreases, reaches a minimum value, and then increases. Conversely, an increase in the values of the parameters  $m_0 > 0$  or  $m_2 > 0$ , with the other parameters held constant, results in an increase in the value of the lensing coefficient  $\bar{b}$  (see Table II). The lensing coefficient  $\bar{b}$  reaches the value  $\bar{b} = -0.40023$  [56] when both  $S_0 \rightarrow 0$  and  $S_2 \rightarrow 0$ , corresponding to Schwarzschild black hole.

The behavior of the strong deflection angle,  $\alpha_D$ , is expressed as a function of the parameter pairs  $(S_0, S_2)$  and  $(m_0, m_2)$  (see Fig. 7). It is observed from Fig. 7 that as the numerical values of the parameters  $S_0 > 0$  or  $S_2 > 0$  increase while keeping the other parameters fixed, the lensing coefficient  $\bar{a}$  increases. Similarly, an increase in the values of the parameters  $m_0 > 0$  or  $m_2 > 0$ , with the other parameters held constant, decreases the value of the strong deflection angle,  $\alpha_D$ . Fig. 7 also shows that  $\alpha_D \rightarrow \infty$  as  $u \rightarrow u_{ph}$ , i.e., the strong deflection angle  $\alpha_D$  unboundedly large when  $u \rightarrow u_{ph}$ . Furthermore, the strong deflection angle,  $\alpha_D$ , in the context of an asymptotically safe quantum gravity black hole is more significant than that of a Schwarzschild black hole. The asymptotically safe quantum gravity black hole, with the presence of parameters  $S_0, S_2, m_0$ , and  $m_2$ , can significantly intensify the gravitational lensing effect compared to other black holes. This result indicates that the gravitational lensing effect produced by an asymptotically safe quantum gravity black hole is significantly enhanced compared to ordinary astrophysical black holes such as the Schwarzschild black hole ( $S_0 = S_2 = 0$ ). Thus, the asymptotically safe quantum gravity black hole, influenced by moving fluids and sound waves, can be detected more quickly and distinguished from ordinary astrophysical black holes, such as the Schwarzschild black hole.

### B. Lensing observables

We now turn to exploring the observable features of strong gravitational lensing within the framework of asymptotically safe quantum gravity black hole geometry. In this analysis, we assume that both the observer and the source are positioned at large distances from the black hole (acting as the lens) with near-perfect alignment. Furthermore, the source is assumed to lie directly behind the black hole. Under these conditions, the lens equation is expressed as [121]

$$\beta = \theta - \frac{D_{ls}}{D_{os}} \Delta \alpha_n. \quad (26)$$

where  $\Delta \alpha_n = \alpha_D(\theta) - 2n\pi$  denotes the offset deflection angle, with  $\alpha_D(\theta)$  representing the primary deflection angle, and  $n$  indicating the number of loops or revolutions a photon completes around the black hole. The angles  $\beta$  and  $\theta$  correspond to the angular separations between the lens (black hole) and the source and between the image and the source, respectively. The distances  $D_{ol}$ ,  $D_{ls}$ , and  $D_{os}$  refer to the observer-lens, lens-source, and observer-source distances, respectively, with the relation  $D_{os} = D_{ol} + D_{ls}$ .

From Eqs. (21) and (26), the angular separation between the black hole (lens) and the  $n^{\text{th}}$  relativistic image is given by

$$\theta_n = \theta_n^0 - \frac{u_{ph} e_n (\theta_n^0 - \beta) D_{os}}{\bar{a} D_{ol} D_{ls}}. \quad (27)$$

Here,  $\theta_n^0$  denotes the angular position of the image corresponding to a photon completing  $2n\pi$  rotations around the black hole (lens). In the framework of strong gravitational lensing, where surface brightness remains conserved, the magnification of the relativistic effect is defined as the ratio of the solid angle subtended by the  $n^{\text{th}}$  image to that subtended by the source [49].

The magnification for the  $n^{\text{th}}$  relativistic image is given by [56]

$$\mu_n = \left( \frac{\beta}{\theta} \frac{d\beta}{d\theta} \right)^{-1} \Big|_{\theta_n^0} = \frac{u_{ph}^2 (1 + e_n) e_n D_{os}}{\beta \bar{a} D_{ls} D_{ol}^2}. \quad (28)$$

The above equation indicates that the first relativistic image exhibits the highest brightness, with the magnification decreasing exponentially as  $n$  increases. In other words, the brightness of the first image exceeds that of the subsequent relativistic images. Moreover, Eq. (27) becomes unbounded as  $\beta \rightarrow 0$ , implying that perfect alignment enhances the chances of detecting relativistic images.

We focus on the scenario where the brightest image, i.e., the outermost image at  $\theta_1$ , is resolved as a distinct image, while the remaining inner images cluster near  $\theta_\infty$ , defined as  $\theta_n|n \rightarrow \infty := \theta_\infty$ . Utilizing the deflection angle from Eq. (22), one can derive key strong lensing observables, including the angular position of the image cluster at  $\theta_\infty$ , the angular separation  $S$  between the outermost and innermost images, and the relative magnification  $r_{mag}$  between the outermost and inner relativistic images. These quantities are given as [56, 64]:

$$\theta_\infty = \frac{u_{ph}}{D_{ol}}, \quad (29)$$

$$X = \theta_1 - \theta_\infty \approx \theta_\infty e^{\frac{(\bar{b}-2\pi)}{\bar{a}}}, \quad (30)$$

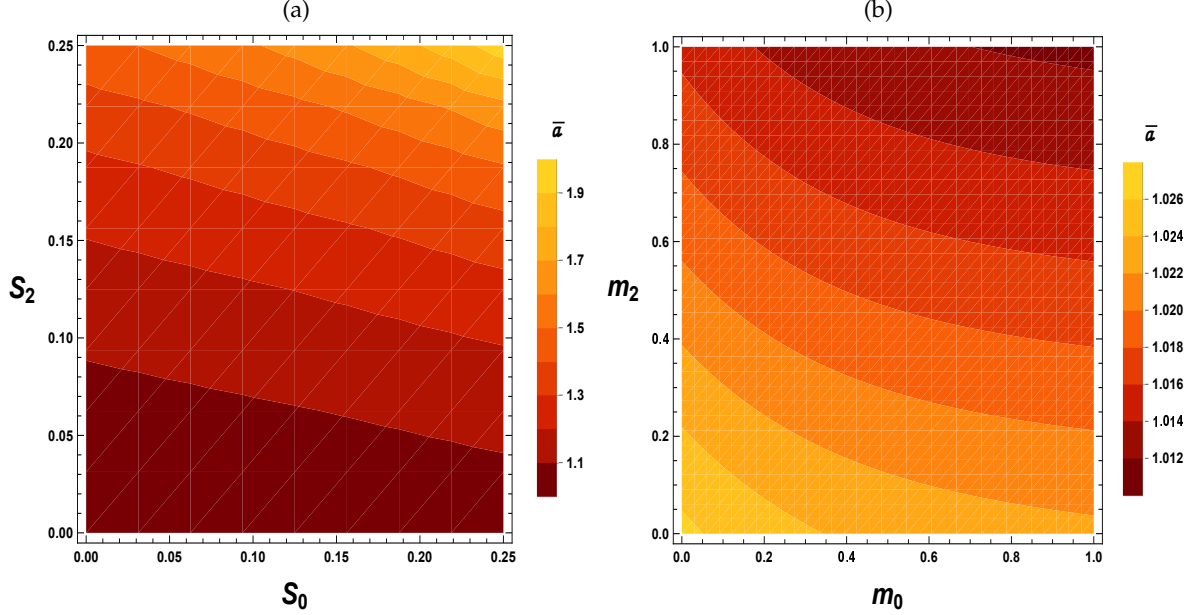


FIG. 5: The deflection angle coefficient  $\bar{a}$  is presented as a function of the parameters  $S_0$ ,  $S_2$  and  $m_0$ ,  $m_2$ .

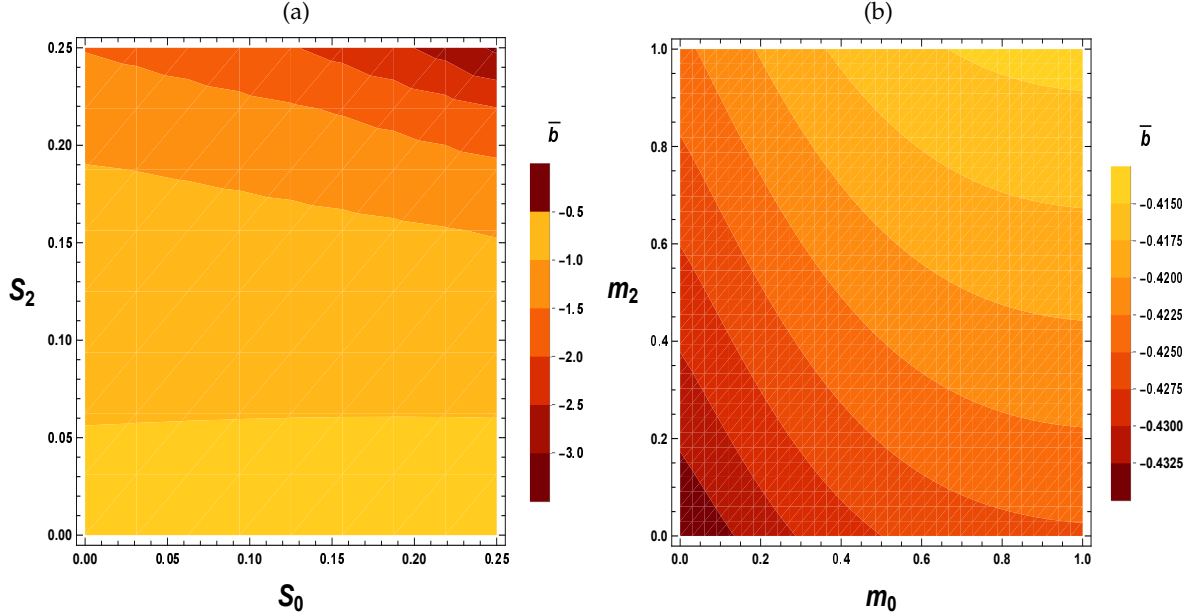


FIG. 6: The deflection angle coefficient  $\bar{b}$  is presented as a function of the parameters  $S_0$ ,  $S_2$  and  $m_0$ ,  $m_2$ .

$$r_{mag} = \frac{\mu_1}{\sum_{n=2}^{\infty} \mu_n} \approx \frac{5\pi}{\bar{a} \log(10)}. \quad (31)$$

If the strong lensing observables  $\theta_\infty$ ,  $X$ , and  $r_{mag}$  are determined from observations, the lensing coefficients  $\bar{a}$ ,  $\bar{b}$ , and the minimum impact parameter  $u_{ph}$  can be computed by inverting Eqs. (29), (30), and (31), respectively. Additionally, the observed data can be compared with the corresponding theoretical predictions. These results enable the identification and distinction of the

asymptotically safe quantum gravity black hole from a Schwarzschild black hole.

### 1. *Lensing observables and the asymptotically safe quantum gravity black hole parameters*

Considering the supermassive black holes  $M87^*$  and  $SgrA^*$  in the center of the nearby galaxies, we numer-

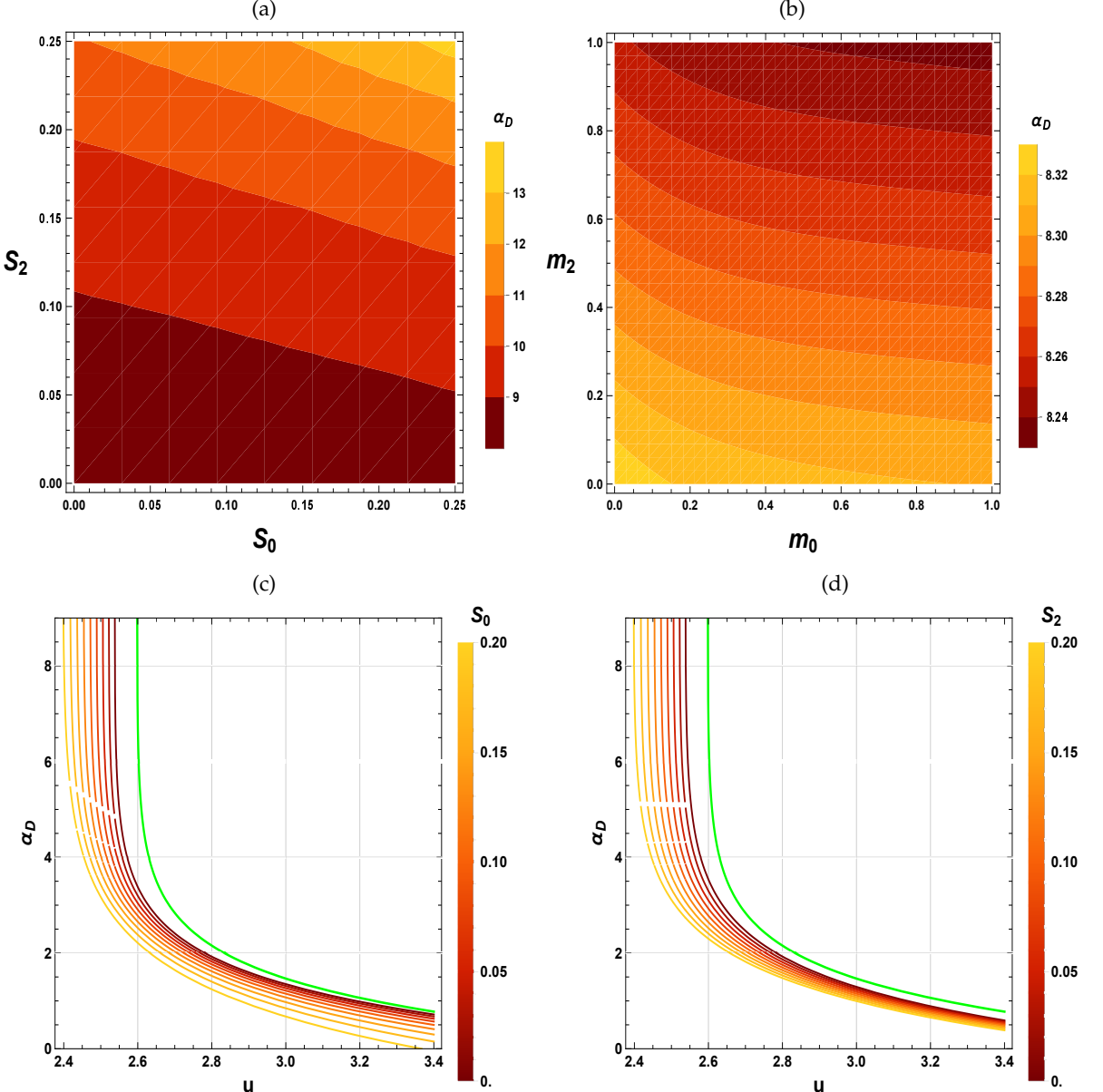


FIG. 7: (a), (b) The strong deflection angle  $\alpha_D$  is shown as a function of the parameters  $S_0, S_2$  and  $m_0, m_2$ . (c), (d) The strong deflection angle  $\alpha_D$  is presented as a function of the impact parameter  $u$ , where the deflection angle diverges as  $u \rightarrow r_{ph}$ . The green curve corresponds to Schwarzschild black hole ( $S_0 = S_2 = 0$ ).

ically obtain the observable quantities  $\theta_\infty, X$  and  $r_{mag}$  for the asymptotically safe quantum gravity black hole (see Table III). The mass and distance from the earth for *M87\** [5] are  $M \approx 6.5 \times 10^9 M_\odot, D_{ol} \approx 16.8 \text{ Mpc}$ , for *SgrA\** are  $M \approx 4.28 \times 10^6 M_\odot, D_{ol} \approx 8.32 \text{ kpc}$  [122]. The behavior of the observable quantities  $\theta_\infty, X$  and  $r_{mag}$  for the supermassive black holes *M87\** and *SgrA\** are expressed as functions of the parameter pairs  $(S_0, S_2)$  and  $(m_0, m_2)$  (see Figs. 8, 9 and 10). It is observed from Fig. 8 that as the numerical values of the parameters  $S_0 > 0$  or  $S_2 > 0$  increase while keeping the other parameters

fixed, the observable quantity  $\theta_\infty$  decreases. Similarly, an increase in the values of the parameters  $m_0 > 0$  or  $m_2 > 0$ , with the other parameters held constant, also increases the value of the observable quantity  $\theta_\infty$  (see Table III). The observable quantity  $\theta_\infty$  reaches the maximum value when both  $S_0 \rightarrow 0$  and  $S_2 \rightarrow 0$ , corresponding to Schwarzschild black hole. Furthermore, Fig. 9 shows that as the numerical values of the parameters  $S_0 > 0$  or  $S_2 > 0$  increase, while keeping the other parameters fixed,  $X$  increases. Conversely, an increase in the values of the parameters  $m_0 > 0$  or  $m_2 > 0$ ,

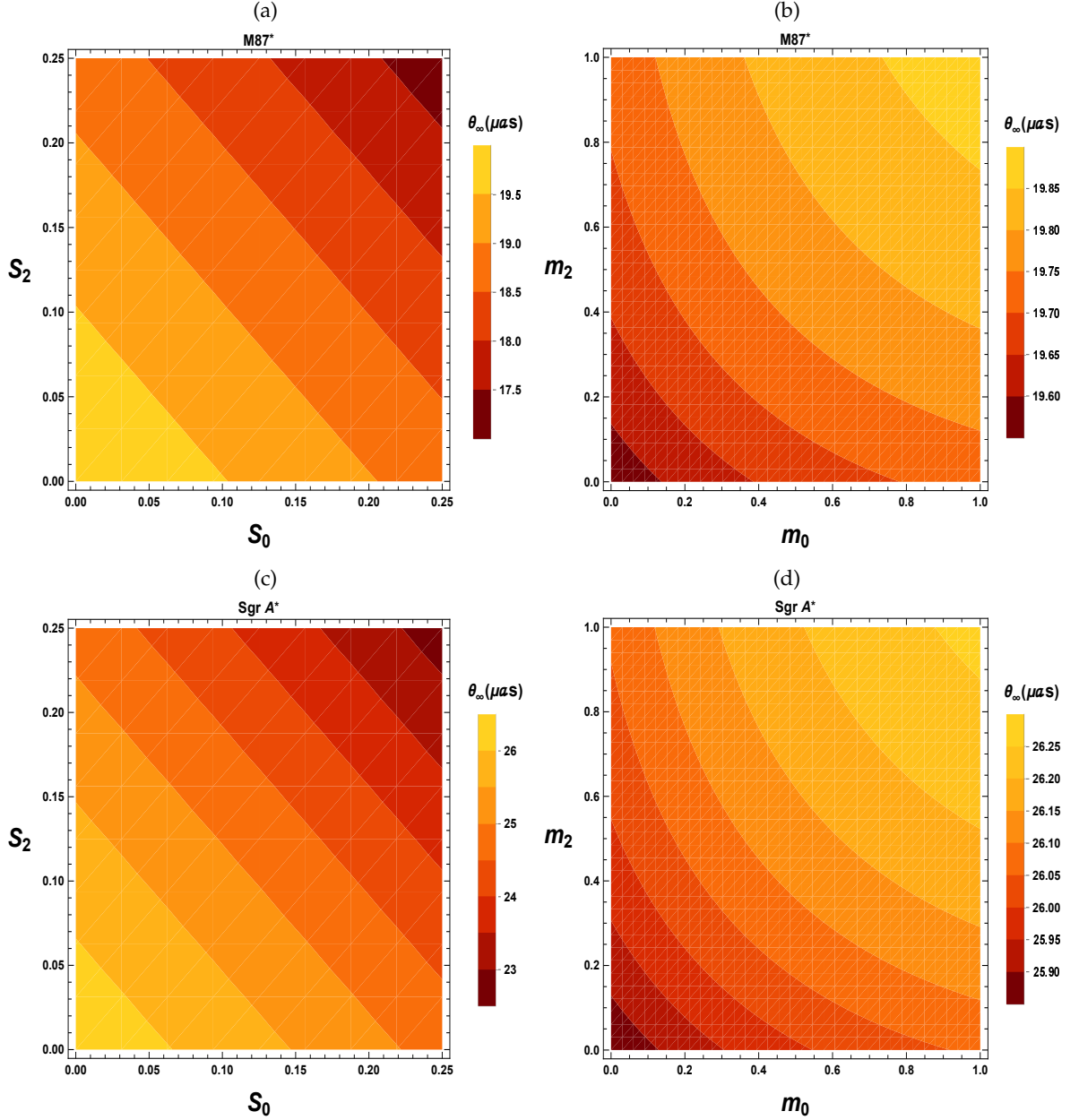


FIG. 8: The angular position of the images  $\theta_\infty$  ( $\mu\text{as}$ ) is presented as a function of the parameters  $S_0$ ,  $S_2$  and  $m_0$ ,  $m_2$ .

with the other parameters held constant, results in a decrease in the value of the observable quantity  $X$  (see Table III). The observable quantity  $X$  reaches the minimum value when both  $S_0 \rightarrow 0$  and  $S_2 \rightarrow 0$ , corresponding to Schwarzschild black hole.

It is also observed from Fig. 10 that as the numerical values of the parameters  $S_0 > 0$  or  $S_2 > 0$  increase while keeping the other parameters fixed, the observable quantity  $r_{\text{mag}}$  decreases. Similarly, an increase in the values of the parameters  $m_0 > 0$  or  $m_2 > 0$ , with the other parameters held constant, also increases the

value of the observable quantity  $r_{\text{mag}}$  (see Table III). The observable quantity  $r_{\text{mag}}$  reaches the maximum value when  $S_0 \rightarrow 0$  and  $S_2 \rightarrow 0$  correspond to Schwarzschild's black hole.

It is also observed that the relative magnification  $r_{\text{mag}}$  of the relativistic images remains independent of the black hole's mass and distance.

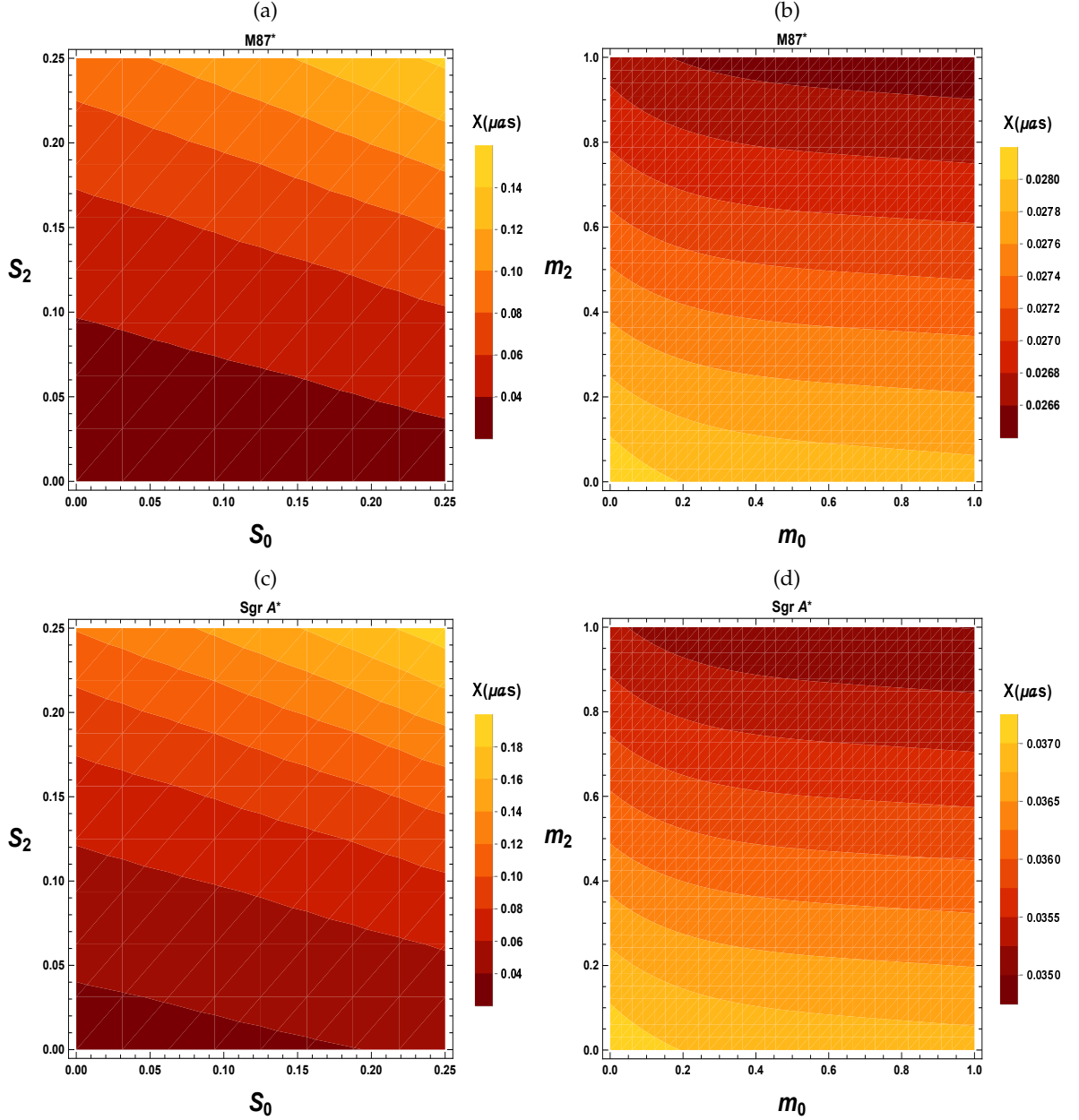


FIG. 9: The angular separation of the images  $X(\mu\text{as})$  is presented as a function of the parameters  $S_0$ ,  $S_2$  and  $m_0$ ,  $m_2$ .

### C. Einstein rings

When the source, the black hole (lens), and the observer are perfectly aligned, corresponding to  $\beta = 0$ , the black hole deflects light rays in all directions, producing a ring-shaped image. This phenomenon, known as the Einstein ring, has been extensively studied in [47, 123–127]. By simplifying Eq. (27) for  $\beta = 0$ , the angular radius of the  $n^{\text{th}}$  relativistic image can be expressed as

$$\theta_n = \theta_n^0 \left( 1 - \frac{u_{ph} e_n D_{os}}{\bar{a} D_{ls} D_{ol}} \right). \quad (32)$$

In the scenario where the black hole (lens) is positioned at a distance halfway between the source and the observer, denoted as  $D_{os} = 2D_{ol}$ , and assuming that  $D_{ol} \gg u_{ph}$ , the angular radius of the  $n^{\text{th}}$  relativistic Einstein ring within the spacetime of an asymptotically safe quantum gravity black hole can be expressed as follows

$$\theta_n^E = \frac{u_{ph}(1 + e_n)}{D_{ol}}. \quad (33)$$

The angular radius  $\theta_1^E$  represents the outermost Einstein ring, as displayed in Fig. 11 for the supermassive

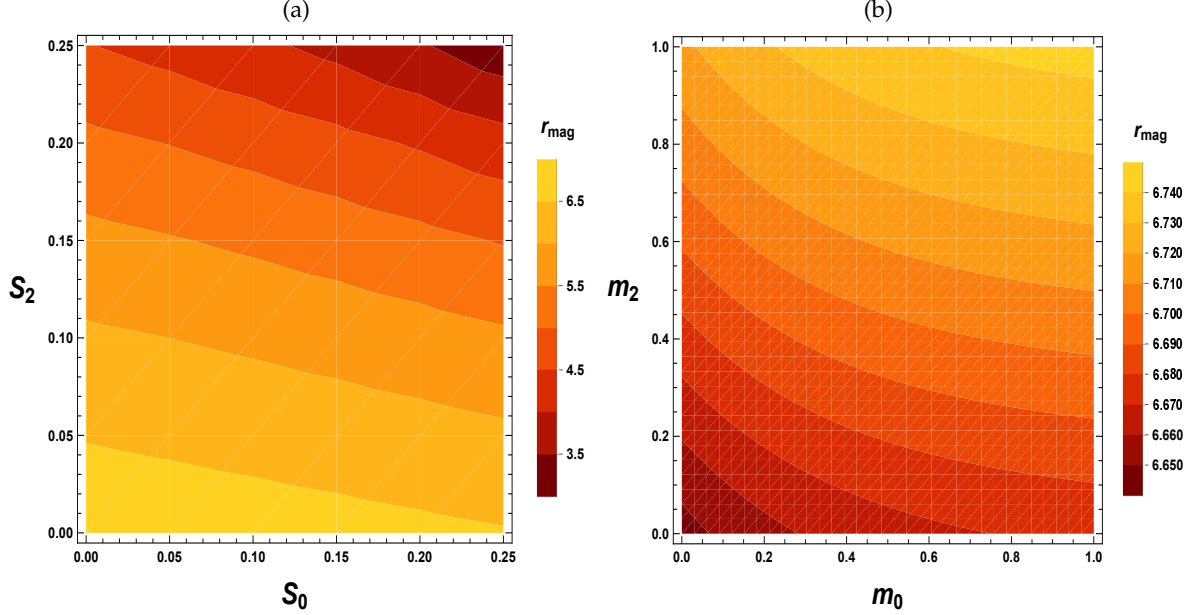


FIG. 10: The relative magnification of the images  $r_{mag}$  is presented as a function of the parameters  $S_0$ ,  $S_2$  and  $m_0$ ,  $m_2$ .

black holes  $M87^*$  and  $SgrA^*$ . From Fig. 11, it is observed that the angular radius  $\theta_1^E$  of the outermost Einstein ring decreases with the increasing value of the parameter  $S_0$  or parameter  $S_2$ . From Fig. 11, it is also evident that the angular radius  $\theta_1^E$  of the outermost Einstein ring for the asymptotically safe quantum gravity black hole is smaller than the corresponding angular radius of the Schwarzschild black hole.

#### D. Time delay in the strong field limit

Time delay is one of the most significant observables in the strong gravitational lensing effect. It arises from the time difference between the formation of two relativistic images. This time difference occurs because the photon traverses different paths around the black hole. Since the travel time for photon paths associated with distinct relativistic images is different, a time difference exists between these images. If the time signals from two relativistic images are obtained through observations, one can calculate the time delay between the two signals [54, 128]. The time taken by a photon to orbit the black hole is given by [128]

$$\tilde{T} = \tilde{a} \log \left( \frac{u}{u_{ph}} - 1 \right) + \tilde{b} + \mathcal{O}(u - u_{ph}). \quad (34)$$

Using the above Eq. (34), one can calculate the time difference between two relativistic images. In the context

of a spherically symmetric static black hole spacetime, the time delay between two relativistic images, when both images are on the same side of the black hole, is expressed as follows

$$\Delta T_{2,1} = 2\pi u_{ph} = 2\pi D_{ol} \theta_\infty. \quad (35)$$

Using the above equation, the time delays for a Schwarzschild black hole ( $S_0 = S_2 = 0$ ) and the asymptotically safe quantum gravity black hole, with  $S_0 = S_2 = 0.1$  and  $m_0 = m_2 = 1$  have been estimated in Table IV for several supermassive black holes located in the centers of nearby galaxies. The deviation of the time delays between the first and second relativistic images, for the asymptotically safe quantum gravity black hole from Schwarzschild black hole  $\delta\Delta T_{2,1} = \Delta T_{2,1}^{Sch} - \Delta T_{2,1}^{ASQG}$  minutes with  $S_0 = S_2 = 0.1$  and  $m_0 = m_2 = 1$  has been displayed for the cases of the supermassive black holes  $M87^*$  and  $SgrA^*$  in Fig. 12. Fig. 12 shows that as the numerical values of the parameters  $S_0 > 0$  or  $S_2 > 0$  increase while keeping the other parameters fixed,  $\delta\Delta T_{2,1}$  increases. Conversely, an increase in the values of the parameters  $m_0 > 0$  or  $m_2 > 0$ , with the other parameters held constant, decreases the value of the observable quantity  $\delta\Delta T_{2,1}$ .

Strong Lensing Coefficients						
$S_0$	$m_0$	$S_2$	$m_2$	$\bar{a}$	$\bar{b}$	$u_{ph}$
0		0		1	-0.40023	2.59808
0.1	0.5	0.1	0.3	1.31945	-1.00257	2.28715
			0.6	1.27941	-0.882235	2.34857
			0.9	1.25713	-0.821543	2.39032
			1.1	1.24752	-0.800193	2.41006
	0.5	0.2	0.3	1.52133	-1.5402	2.09035
			0.6	1.3881	-1.0993	2.21375
			0.9	1.32338	-0.910493	2.30134
			1.1	1.29772	-0.849069	2.34341
	0.5	0.3	0.3	2.03915	-3.44553	1.87746
			0.6	1.58237	-1.60264	2.06229
			0.9	1.42174	-1.08157	2.20068
			1.1	1.36647	-0.936446	2.26848
0.1	1	0.1	0.3	1.20153	-0.753994	2.35682
			0.6	1.17352	-0.675696	2.41898
			0.9	1.15807	-0.638187	2.46065
			1.1	1.15139	-0.626371	2.48013
	1	0.2	0.3	1.33508	-1.04248	2.16208
			0.6	1.24902	-0.78693	2.28751
			0.9	1.20606	-0.676661	2.37513
			1.1	1.18869	-0.643378	2.41666
	1	0.3	0.3	1.61347	-1.84353	1.95072
			0.6	1.37237	-1.02851	2.13973
			0.9	1.27383	-0.753786	2.27858
			1.1	1.23801	-0.678277	2.34553

TABLE II: Estimation of the strong lensing coefficients for different values of the asymptotically safe quantum gravity black hole parameters  $S_0 = 0, 0.1, S_2 = 0, 0.1, 0.2, 0.3, m_0 = 0.5, 1$  and  $m_2 = 0.3, 0.6, 0.9, 1.1$  respectively.

### E. Results and discussions

Using observations of strong gravitational fields, we have applied the methodology introduced by Bozza [56] to distinguish between various types of spherically symmetric black holes and investigate their astrophysical implications, particularly for supermassive black holes located at the centers of nearby galaxies. This methodology has been extensively employed to test the key properties of asymptotically safe quantum gravity black holes and compare them with the standard Schwarzschild general relativity solution. In

our analysis, we investigated several key aspects of astrophysical relevance. First, we computed the strong lensing coefficients  $\bar{a}$ ,  $\bar{b}$ , and  $u_{ph}$  (see Table II). Utilizing these coefficients, we derived the strong deflection angle along with several observable quantities, such as the angular position of the innermost image  $\theta_\infty$ , the image separation  $X$ , and the magnification ratio  $r_{mag}$ , specifically for the supermassive black holes M87 and Sgr A (see Table III). Furthermore, we examined the time delay between relativistic images (see Table IV) for multiple supermassive black holes located at the centers of nearby galaxies.

Parameters				M87*		SgrA*		M87*,SgrA*
$S_0$	$m_0$	$S_2$	$m_2$	$\theta_\infty(\mu\text{as})$	$X(\mu\text{as})$	$\theta_\infty(\mu\text{as})$	$X(\mu\text{as})$	$r_{\text{mag}}$
0		0		19.9632	0.0249839	26.3826	0.0330177	6.82188
0.1	0.5	0.1	0.3	17.5741	0.0702727	23.2252	0.0928695	5.17023
			0.6	18.0461	0.0666955	23.849	0.0881421	5.33203
			0.9	18.3668	0.0645049	24.2729	0.085247	5.42657
			1.1	18.5185	0.0633437	24.4733	0.0837124	5.46834
	0.2	0.5	0.3	16.0619	0.0938527	21.2268	0.124032	4.48417
			0.6	17.0101	0.0833594	22.4799	0.110164	4.91454
			0.9	17.6831	0.0770561	23.3693	0.101834	5.15489
			1.1	18.0064	0.0738842	23.7965	0.0976423	5.25682
	0.3	0.3	0.3	14.4262	0.12222	19.065	0.161522	3.34546
			0.6	15.8463	0.108542	20.9418	0.143445	4.31118
			0.9	16.9097	0.0951575	22.3472	0.125756	4.79827
			1.1	17.4306	0.0884627	23.0356	0.116909	4.99233
0.2	0.1	0.1	0.3	18.1094	0.0517972	23.9327	0.068453	5.67767
			0.6	18.5871	0.0494169	24.5639	0.0653073	5.81319
			0.9	18.9073	0.0479746	24.987	0.0634013	5.89072
			1.1	19.0569	0.0471875	25.1849	0.0623611	5.92491
	0.2	0.5	0.3	16.6131	0.068777	21.9552	0.0908929	5.10973
			0.6	17.5769	0.0611796	23.2289	0.0808525	5.46178
			0.9	18.2502	0.0568936	24.1187	0.0751882	5.65635
			1.1	18.5693	0.0547179	24.5404	0.072313	5.73901
	0.3	0.3	0.3	14.9891	0.0973464	19.8089	0.128649	4.22809
			0.6	16.4413	0.079819	21.7282	0.105486	4.97088
			0.9	17.5083	0.0698379	23.1383	0.0922948	5.3554
			1.1	18.0227	0.065123	23.8181	0.0860639	5.51037

TABLE III: Estimation of the strong lensing observables for the Supermassive Black Holes  $M87^*$ ,  $SgrA^*$  for different values of the asymptotically safe quantum gravity black hole parameters  $S_0 = 0.1, m_0 = 0.5, 1, m_2 = 0.3, 0.6, 0.9, 1.1$  and  $S_2 = 0.1, 0.2, 0.3$  respectively. The observable quantity  $r_{\text{mag}}$  does not depend on the mass or the distance of the black hole from the observer.

a. *Angular position  $\theta_\infty$  for the set of images.* We have numerically determined the angular positions of the relativistic images for various supermassive black holes within the asymptotically safe quantum gravity framework. The results for the supermassive black holes  $M87^*$  and  $SgrA^*$  are summarized in Table V. As one can see from Tables II and V, the angular position of the innermost relativistic images  $\theta_\infty$  depends on the values of the asymptotically safe quantum gravity

black hole parameters  $S_2$ ,  $m_0$ , and  $m_2$ . An increase in the value of  $m_2$  from 0.3 to 1.1 will lead, for the black holes  $M87^*$  and  $SgrA^*$ , to an increase in  $\theta_\infty$  for fixed values of the remaining parameters, while  $\theta_\infty$  decreases with an increase in the parameter  $S_2$  from 0.1 to 0.3, assuming the other parameters are fixed. Furthermore, considering the same mass and distance of the black hole, it is observed that the angular position of the innermost relativistic images  $\theta_\infty$  for the asymptotically safe quantum gravity black hole is smaller than that in

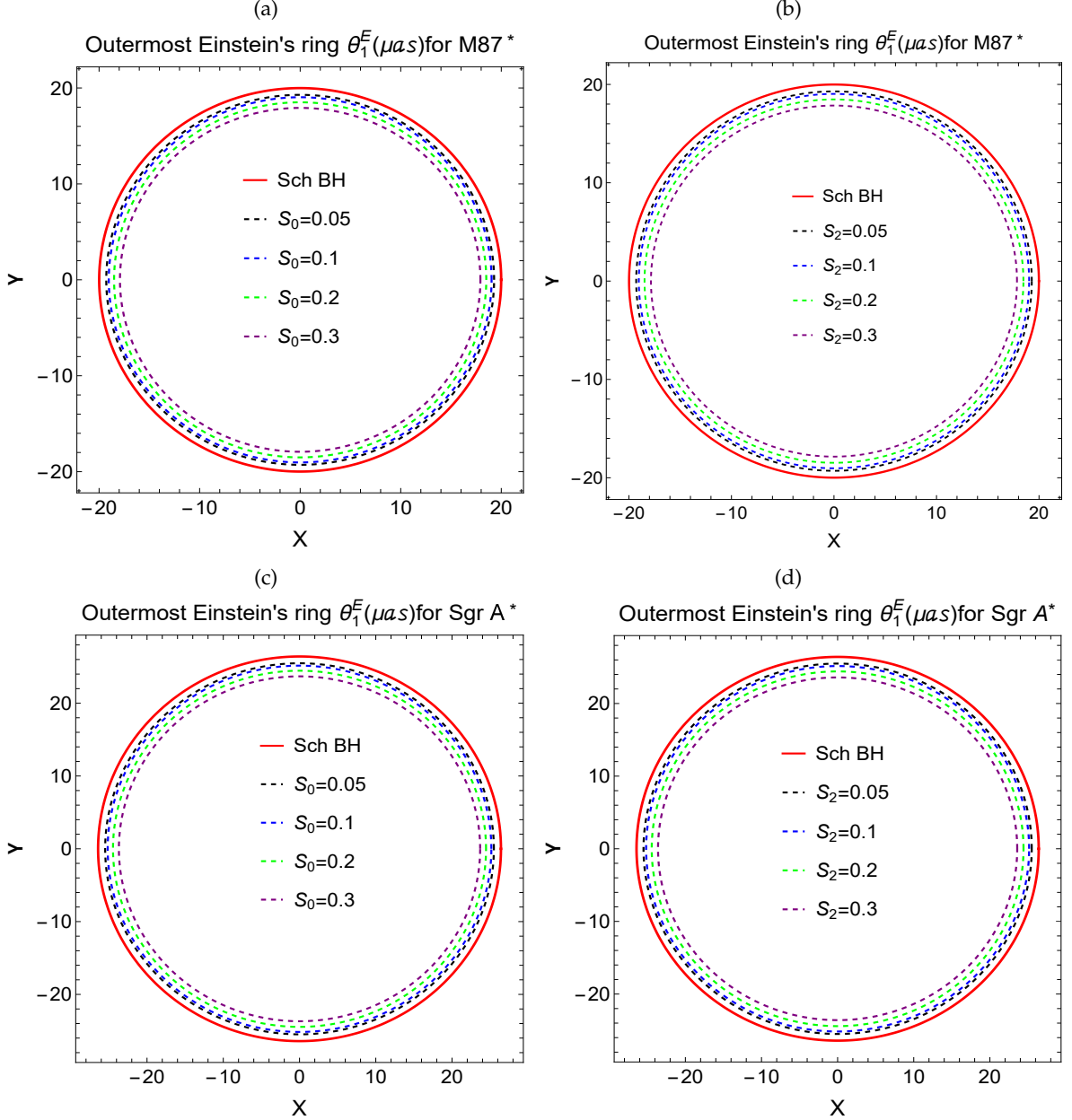


FIG. 11: The outermost Einstein ring  $\theta_1^E$  ( $\mu$ as) of the black hole in asymptotically safe quantum gravity, in the context of  $M87^*$  and  $SgrA^*$ , is presented in the X-Y plane. The black hole parameters  $S_0$  and  $S_2$  are varied independently, while the other parameters remain fixed.

the case of a Schwarzschild black hole. Consequently, the fundamental asymptotically safe theory of quantum gravity has a significant effect on the potentially observable angular positions of the images  $\theta_\infty$ , enabling a distinction between these images and those associated with other classical black holes.

*b. The angular separation.* We have numerically obtained the angular separation between the outermost and innermost relativistic images  $X$  for the supermassive black holes  $M87^*$  and  $SgrA^*$  within the framework of asymptotically safe quantum gravity, as summarized in Table VI.

As one can see from Tables II and VI, the angular separation between outermost and innermost relativistic

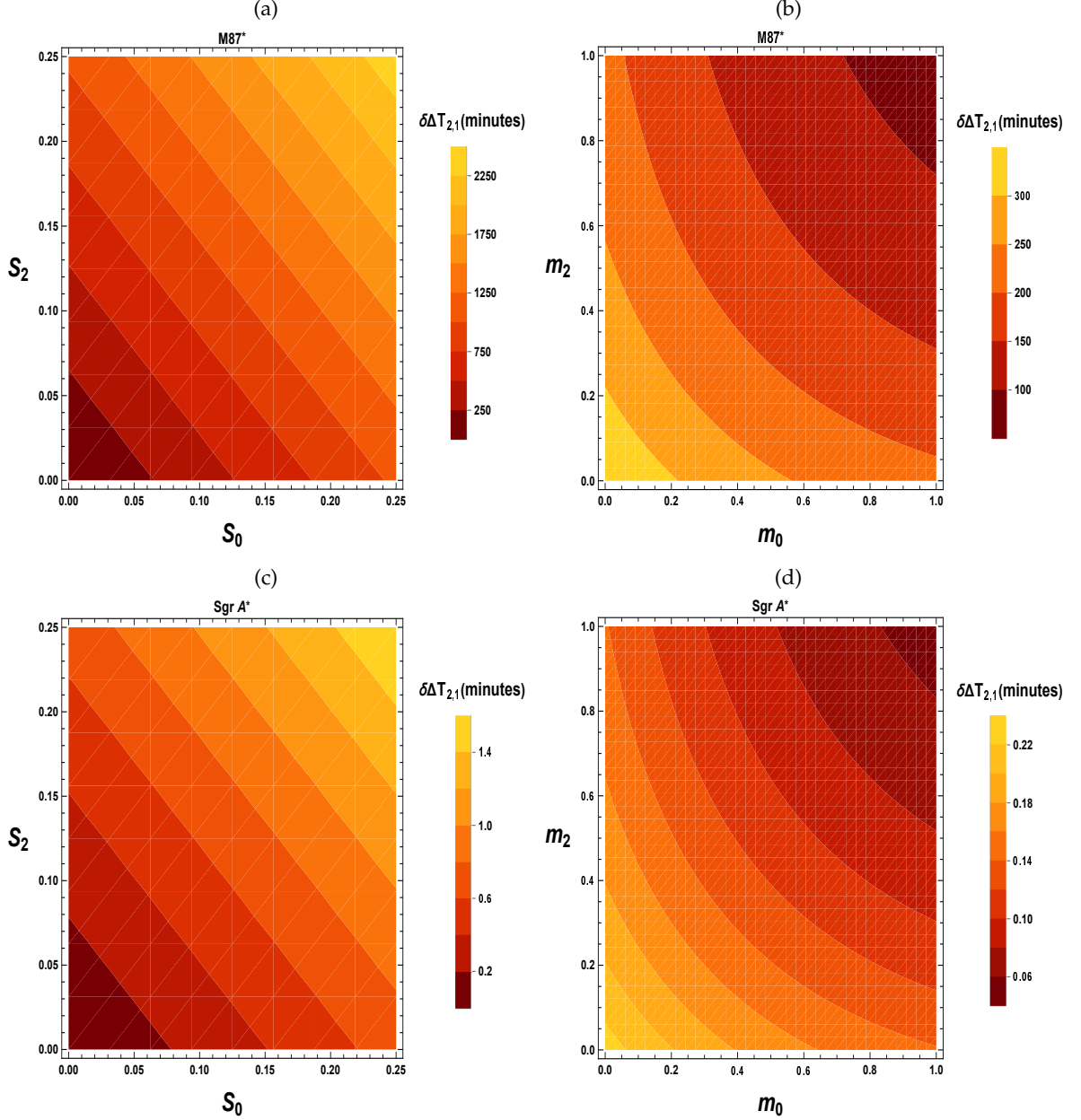


FIG. 12: The deviation of the time delays between the first and second relativistic images, for the asymptotically safe quantum gravity black hole from Schwarzschild black hole  $\delta\Delta T_{2,1} = \Delta T_{2,1}^{Sch} - \Delta T_{2,1}^{ASGQ}$  minutes is presented as a function of the parameters  $S_0$ ,  $S_2$  and  $m_0$ ,  $m_2$ .

images  $X$  depends on the values of the asymptotically safe quantum gravity black hole parameters  $S_2$ ,  $m_0$ , and  $m_2$ . An increase in the value of  $m_2$  from 0.3 to 1.1 will lead, for the black holes  $M87^*$  and  $SgrA^*$ , to a decrease in  $X$  for fixed values of the remaining parameters, while  $X$  increases with an increase in the parameter  $S_2$  from 0.1 to 0.3, assuming the other parameters are fixed. Furthermore, considering the same mass and distance of the black hole, it is observed that the angular separation

between outermost and innermost relativistic images  $X$  for the asymptotically safe quantum gravity black hole is larger than that in the case of a Schwarzschild black hole. Consequently, the fundamental asymptotically safe theory of quantum gravity has a significant effect on the potentially observable angular separation between the outermost and innermost relativistic images  $X$ , enabling a distinction between these images and those associated with other classical black holes.

Galaxy	$M(M_\odot)$	$D_{ol}(Mpc)$	$\Delta T_{2,1}$ Schwarzschild BH ( $S_0 = S_2 = 0$ )	$\Delta T_{2,1}$ ASQG BH ( $S_0 = S_2 = 0.1$ , $m_0 = m_2 = 1$ )
NGC 4395	$3.6 \times 10^5$	4.3	0.962522	0.915472
Milky Way	$4.3 \times 10^6$	0.0083	11.4968	10.9348
NGC 7457	$8.95 \times 10^6$	12.53	23.9294	22.7596
NGC 4486A	$1.44 \times 10^7$	18.36	38.5009	36.6189
NGC 2778	$1.45 \times 10^7$	23.44	38.7682	36.8732
NGC 3607	$1.37 \times 10^8$	22.65	366.293	348.388
NGC 4026	$1.80 \times 10^8$	13.35	481.261	457.736
NGC 5576	$2.73 \times 10^8$	25.68	729.912	694.233
NGC 7052	$3.96 \times 10^8$	70.4	1058.77	1007.02
NGC 3379	$4.16 \times 10^8$	10.70	1112.25	1057.88
NGC 4261	$5.29 \times 10^8$	32.36	1414.37	1345.23
NGC 6251	$6.14 \times 10^8$	108.4	1641.63	1561.39
NGC 5077	$8.55 \times 10^8$	38.7	2285.99	2174.25
NGC 7768	$1.34 \times 10^9$	116.0	3582.72	3407.59
NGC 6861	$2.10 \times 10^9$	28.71	5614.71	5340.25
NGC 4751	$2.44 \times 10^9$	32.81	6523.76	6204.86
Cygnus A	$2.66 \times 10^9$	242.7	7111.95	6764.32
NGC 5516	$3.69 \times 10^9$	55.3	9865.85	9383.59
NGC 4649	$4.72 \times 10^9$	16.46	12619.7	12002.9
M87	$6.5 \times 10^9$	16.68	17378.9	16529.4
NGC 3842	$9.09 \times 10^9$	92.2	24303.7	23115.7

TABLE IV: Estimation of the time delay for various supermassive BHs for the Schwarzschild metric and for the asymptotically safe quantum gravity black holes, respectively. The masses and the distances are expressed in Solar Masses and Mpc units [129]. The time delays  $\Delta T_{2,1}$  are estimated in minutes.

SMBH	$S_0$	$m_0$	$S_2$	$m_2$	$\theta_\infty$ ( $\mu$ as)
$M87^*$	0.1	0.5	0.1	$0.3 \leq m_2 \leq 1.1$	$\theta_\infty \in (17.57, 18.52)$
$SgrA^*$	0.1	0.5	0.1	$0.3 \leq m_2 \leq 1.1$	$\theta_\infty \in (23.22, 24.48)$
$M87^*$	0.1	0.5	0.2	$0.3 \leq m_2 \leq 1.1$	$\theta_\infty \in (16.06, 18.01)$
$SgrA^*$	0.1	0.5	0.2	$0.3 \leq m_2 \leq 1.1$	$\theta_\infty \in (21.22, 23.80)$
$M87^*$	0.1	0.5	0.3	$0.3 \leq m_2 \leq 1.1$	$\theta_\infty \in (14.42, 17.44)$
$SgrA^*$	0.1	0.5	0.3	$0.3 \leq m_2 \leq 1.1$	$\theta_\infty \in (19.06, 23.04)$
$M87^*$	0.1	1	0.1	$0.3 \leq m_2 \leq 1.1$	$\theta_\infty \in (18.10, 19.06)$
$SgrA^*$	0.1	1	0.1	$0.3 \leq m_2 \leq 1.1$	$\theta_\infty \in (23.93, 25.19)$
$M87^*$	0.1	1	0.2	$0.3 \leq m_2 \leq 1.1$	$\theta_\infty \in (16.61, 18.57)$
$SgrA^*$	0.1	1	0.2	$0.3 \leq m_2 \leq 1.1$	$\theta_\infty \in (21.95, 24.55)$
$M87^*$	0.1	1	0.3	$0.3 \leq m_2 \leq 1.1$	$\theta_\infty \in (14.98, 18.03)$
$SgrA^*$	0.1	1	0.3	$0.3 \leq m_2 \leq 1.1$	$\theta_\infty \in (19.80, 23.82)$

TABLE V: Admissible range for the angular position of the innermost relativistic images  $\theta_\infty$ , is analyzed for the supermassive black holes  $M87^*$  and  $SgrA^*$ . This range is determined for varying values of the asymptotically safe quantum gravity black hole parameters  $S_2$ ,  $m_0$ , and  $m_2$  while keeping the parameter  $S_0$  constant.

c. *Relative magnification.* We have numerically obtained the relative magnification of the relativistic images  $r_{mag}$  for the supermassive black holes  $M87^*$  and

$SgrA^*$  within the framework of asymptotically safe quantum gravity, as summarized in Table VII.

As illustrated in Tables II and VII, the relative magnification of the relativistic images, denoted as  $r_{mag}$ , is influenced by the parameters of the asymptotically safe quantum gravity black hole, specifically  $S_2$ ,  $m_0$ , and  $m_2$ . Increasing the value of  $m_2$  from 0.3 to 1.1 results in a corresponding rise in  $r_{mag}$  for the supermassive black holes  $M87^*$  and  $SgrA^*$ , assuming the other parameters remain constant. Conversely,  $r_{mag}$  decreases as the parameter  $S_2$  increases from 0.1 to 0.3, again with other parameters held fixed.

Moreover, when comparing black holes of the same mass and distance, it is found that the relative magnification  $r_{mag}$  for the asymptotically safe quantum gravity black hole is less than that for a Schwarzschild black hole. This indicates that the fundamental aspects of asymptotically safe quantum gravity significantly affect the observable relative magnification of the relativistic images, allowing for differentiation between these images and those linked to other classical black holes. It is also important to note that the relative magnification of the relativistic images is independent of the black hole's mass or distance.

SMBH	$S_0$	$m_0$	$S_2$	$m_2$	$X$ ( $\mu$ as)
$M87^*$	0.1	0.5	0.1	$0.3 \leq m_2 \leq 1.1$	$X \in (0.06, 0.08)$
$SgrA^*$	0.1	0.5	0.1	$0.3 \leq m_2 \leq 1.1$	$X \in (0.08, 0.10)$
$M87^*$	0.1	0.5	0.2	$0.3 \leq m_2 \leq 1.1$	$X \in (0.07, 0.10)$
$SgrA^*$	0.1	0.5	0.2	$0.3 \leq m_2 \leq 1.1$	$X \in (0.09, 0.13)$
$M87^*$	0.1	0.5	0.3	$0.3 \leq m_2 \leq 1.1$	$X \in (0.08, 0.13)$
$SgrA^*$	0.1	0.5	0.3	$0.3 \leq m_2 \leq 1.1$	$X \in (0.11, 0.17)$
$M87^*$	0.1	1	0.1	$0.3 \leq m_2 \leq 1.1$	$X \in (0.04, 0.06)$
$SgrA^*$	0.1	1	0.1	$0.3 \leq m_2 \leq 1.1$	$X \in (0.06, 0.07)$
$M87^*$	0.1	1	0.2	$0.3 \leq m_2 \leq 1.1$	$X \in (0.05, 0.07)$
$SgrA^*$	0.1	1	0.2	$0.3 \leq m_2 \leq 1.1$	$X \in (0.07, 0.10)$
$M87^*$	0.1	1	0.3	$0.3 \leq m_2 \leq 1.1$	$X \in (0.06, 0.10)$
$SgrA^*$	0.1	1	0.3	$0.3 \leq m_2 \leq 1.1$	$X \in (0.08, 0.13)$

TABLE VI: Admissible range for the angular separation between outermost and innermost relativistic images  $X$ , is analyzed for the supermassive black holes  $M87^*$  and  $SgrA^*$ . This range is determined for varying values of the asymptotically safe quantum gravity parameters  $S_2$ ,  $m_0$ , and  $m_2$  while keeping the parameter  $S_0$  constant.

SMBH	$S_0$	$m_0$	$S_2$	$m_2$	$r_{mag}$ magnitude
$M87^*, SgrA^*$	0.1	0.5	0.1	$0.3 \leq m_2 \leq 1.1$	$r_{mag} \in (5.17, 5.47)$
$M87^*, SgrA^*$	0.1	0.5	0.2	$0.3 \leq m_2 \leq 1.1$	$r_{mag} \in (4.48, 5.26)$
$M87^*, SgrA^*$	0.1	0.5	0.3	$0.3 \leq m_2 \leq 1.1$	$r_{mag} \in (3.34, 5.00)$
$M87^*, SgrA^*$	0.1	1	0.1	$0.3 \leq m_2 \leq 1.1$	$r_{mag} \in (5.67, 5.93)$
$M87^*, SgrA^*$	0.1	1	0.2	$0.3 \leq m_2 \leq 1.1$	$r_{mag} \in (5.10, 5.74)$
$M87^*, SgrA^*$	0.1	1	0.3	$0.3 \leq m_2 \leq 1.1$	$r_{mag} \in (4.22, 5.52)$

TABLE VII: Admissible range for the relative magnification of the relativistic images  $r_{mag}$ , is analyzed for the supermassive black holes  $M87^*$  and  $SgrA^*$ . This range is determined for varying values of the asymptotically safe quantum gravity parameters  $S_2$ ,  $m_0$ , and  $m_2$  while keeping the parameter  $S_0$  constant.

*d. The Einstein rings.* For the supermassive black holes  $M87^*$  and  $SgrA^*$ , the outermost Einstein rings  $\theta_1^E$  are presented in Figs. 11(a) and 11(c) for the parameter values  $m_0 = m_2 = 1$ ,  $S_0 = 0.1$ , and  $S_2 = 0, 0.05, 0.1, 0.2$ , & 0.3. Additionally, the cases with  $m_0 = m_2 = 1$ ,  $S_2 = 0.1$ , and  $S_0 = 0, 0.05, 0.1, 0.2$ , & 0.3 are shown in Figs. 11(b) and 11(d). Our findings indicate that the radius of the outermost Einstein ring,  $\theta_1^E$ , decreases as the values of the asymptotically safe quantum gravity black hole parameters  $S_0$  or  $S_2$  increase while keeping the remaining parameters fixed. Notably, the Einstein ring  $\theta_1^E$  for an asymptotically safe

quantum gravity black hole is significantly smaller than that of the standard classical Schwarzschild black hole ( $S_0 = S_2 = 0$ ).

*e. Relativistic time delay.* We have also evaluated the time delays  $\Delta T_{2,1}$  between the first and second-order relativistic images for various supermassive black holes within the framework of the asymptotically safe quantum gravity black hole, using the parameter values ( $S_0 = S_2 = 0.1$ ,  $m_0 = m_2 = 1$ ), as well as for the Schwarzschild black hole ( $S_0 = S_2 = 0$ ). The time delay  $\Delta T_{2,1}$  for the asymptotically safe quantum gravity black hole (e.g.,  $\sim 23115.7$  minutes for NGC 3842) is significantly smaller compared to the Schwarzschild black hole (e.g.,  $\sim 24303.7$  minutes for NGC 3842). Thus, the deviation in the time delays for the asymptotically safe quantum gravity black hole with ( $S_0 = S_2 = 0.1$ ,  $m_0 = m_2 = 1$ ) from the standard Schwarzschild black hole ( $S_0 = S_2 = 0$ ) is  $\delta \Delta T_{2,1} = \Delta T_{2,1}^{Sch} - \Delta T_{2,1}^{ASQG} = 1188$  minutes. This suggests that if the first and second relativistic images are distinguishable, the time delay between them could serve as a valuable indicator to differentiate the asymptotically safe quantum gravity black hole from the classical Schwarzschild black hole.

## V. CONCLUSIONS, AND FINAL REMARKS

In the present paper, we have discussed the shadow and strong gravitational lensing phenomena by the asymptotically safe quantum gravity black holes, described by a solution obtained by the quantum effective action and the respective quantum equations of motion from multi-graviton correlation functions in asymptotically safe quantum gravity [101]. A black hole in asymptotically safe quantum gravity is described by five parameters, with  $M$  representing the mass of the black hole. The two free parameters  $S_0$  and  $S_2$  characterize the strength of the exponentially decaying Yukawa corrections. Additionally, the masses  $m_0$  and  $m_2$  of the spin-0 and spin-2 modes are associated with various curvature terms' couplings. This has been discussed in detail in [101]. The classical Schwarzschild black hole is obtained when  $S_0 = S_2 = 0$ . The present study highlights that traditional black hole solutions derived from classical general relativity may not fully capture the complexities of black holes in the context of quantum gravity. The asymptotic safety scenario suggests that gravitational interactions approach a fixed point at high energy scales, indicating new physics beyond classical theories. Quantum black hole solutions

exhibit significant deviations from classical predictions, particularly outside the event horizon. These deviations could manifest in gravitational lensing phenomena, where the curvature of spacetime influences the paths of light rays passing near massive objects. In this study, we primarily restrict our analysis to positive values of the black hole parameters  $S_0, S_2, m_0$ , and  $m_2$ . The study of light deflection (gravitational lensing) in the strong field limit, particularly in regions dominated by the gravitational effects of asymptotically safe quantum gravity black holes, offers powerful theoretical and observational tools for distinguishing between standard general relativistic models and modified gravity models. Although the radial coordinate dependence of the asymptotically safe quantum gravity metric takes a fixed form, when interpreted as a galactic metric, the bending angle of light and other optical effects are significantly influenced by the metric parameters, as well as by the baryonic mass and radius of the supermassive black hole. The asymptotically safe quantum gravity metric dictates the specific values of the bending angles and other lensing effects, and these values differ substantially from those predicted by the classical Schwarzschild metric. For example, when  $S_0 = 0.1, S_2 = 0.1, m_0 = 1$ , and  $m_2 = 1$ , the time delay of the photons is much smaller in the asymptotically safe quantum gravity than in standard general relativity. This may be related to the gravitational light

deflection angle being larger than the value predicted by the standard general relativistic approach. We observe significant differences in the lensing effects when comparing our results for the asymptotically safe quantum gravity black holes with those of standard Schwarzschild black holes. As a result, the asymptotically safe quantum gravity black hole, influenced by moving fluids and sound waves, can be detected more easily and distinguished from ordinary astrophysical black holes, such as the Schwarzschild black hole. Consequently, the study of gravitational lensing may provide evidence for the existence of asymptotically safe quantum gravity effects in the Universe. Our findings represent a promising and significant step toward connecting the fundamental theory of asymptotically safe quantum gravity to potentially feasible black hole spacetimes.

## ACKNOWLEDGEMENTS

FR would like to thank the authorities of the Inter-University Centre for Astronomy and Astrophysics, Pune, India for providing research facilities. This work is a part of the project submitted in DST-SERB, Govt. of India. N.U.M would like to thank CSIR, Govt. of India for providing Senior Research Fellowship (No. 08/003(0141)/2020-EMR-I).

---

[1] K. Schwarzschild, *Sitzungsber. Preuss. Akad. Wiss. Berlin (Math. Phys.)* **1916**, 189 (1916), [arXiv:physics/9905030](https://arxiv.org/abs/physics/9905030).

[2] R. P. Kerr, *Phys. Rev. Lett.* **11**, 237 (1963).

[3] B. P. Abbott *et al.* (LIGO Scientific, Virgo), *Phys. Rev. Lett.* **116**, 061102 (2016), [arXiv:1602.03837 \[gr-qc\]](https://arxiv.org/abs/1602.03837).

[4] K. Akiyama *et al.* (Event Horizon Telescope), *Astrophys. J. Lett.* **930**, L15 (2022).

[5] K. Akiyama *et al.* (Event Horizon Telescope), *Astrophys. J. Lett.* **875**, L1 (2019), [arXiv:1906.11238 \[astro-ph.GA\]](https://arxiv.org/abs/1906.11238).

[6] N. D. Birrell and P. C. W. Davies, *Quantum Fields in Curved Space*, Cambridge Monographs on Mathematical Physics (Cambridge University Press, Cambridge, UK, 1982).

[7] O. Aharony and T. Banks, *Journal of High Energy Physics* **1999**, 016–016 (1999).

[8] J. Kumar, S. U. Islam, and S. G. Ghosh, *Eur. Phys. J. C* **83**, 1014 (2023), [arXiv:2305.04336 \[gr-qc\]](https://arxiv.org/abs/2305.04336).

[9] A. Anjum, M. Afrin, and S. G. Ghosh, *Phys. Dark Univ.* **40**, 101195 (2023), [arXiv:2301.06373 \[gr-qc\]](https://arxiv.org/abs/2301.06373).

[10] L.-M. Cao, L.-B. Wu, Y. Zhao, and Y.-S. Zhou, *Phys. Rev. D* **108**, 124023 (2023).

[11] M. Reuter, *Phys. Rev. D* **57**, 971 (1998), [arXiv:hep-th/9605030](https://arxiv.org/abs/hep-th/9605030).

[12] P. van Nieuwenhuizen, *Physics Reports* **68**, 189 (1981).

[13] S. Weinberg, “ULTRAVIOLET DIVERGENCES IN QUANTUM THEORIES OF GRAVITATION,” in *General Relativity: An Einstein Centenary Survey* (1980) pp. 790–831.

[14] M. Reuter, *Phys. Rev. D* **57**, 971 (1998).

[15] W. Souma, *Prog. Theor. Phys.* **102**, 181 (1999), [arXiv:hep-th/9907027](https://arxiv.org/abs/hep-th/9907027).

[16] O. Lauscher and M. Reuter, *Phys. Rev. D* **65**, 025013 (2001).

[17] K. S. Stelle, *Phys. Rev. D* **16**, 953 (1977).

[18] D. BENEDETTI, P. F. MACHADO, and F. SAUERESSIG, *Modern Physics Letters A* **24**, 2233–2241 (2009).

[19] M. R. Niedermaier, *Phys. Rev. Lett.* **103**, 101303 (2009).

[20] H. Kawai, Y. Kitazawa, and M. Ninomiya, *Nuclear Physics B* **404**, 684 (1993).

[21] K. FALLS, D. F. LITIM, and A. RAGHURAMAN, *International Journal of Modern Physics A* **27**, 1250019 (2012).

[22] A. Bonanno and M. Reuter, *Phys. Rev. D* **62**, 043008 (2000).

[23] M. Reuter, *Physical Review D* **57**, 971–985 (1998).

[24] M. Reuter and F. Saueressig, *Quantum Gravity and the Functional Renormalization Group: The Road towards Asymptotic Safety*, Cambridge Monographs on Mathematical Physics (Cambridge University Press, 2019).

[25] A. Bonanno, A. Eichhorn, H. Gies, J. M. Pawłowski, R. Percacci, M. Reuter, F. Saueressig, and G. P. Vacca, *Front. in Phys.* **8**, 269 (2020), arXiv:2004.06810 [gr-qc].

[26] J. M. Pawłowski and M. Reichert, *Front. in Phys.* **8**, 551848 (2021), arXiv:2007.10353 [hep-th].

[27] E. H. T. Collaboration *et al.*, arXiv preprint arXiv:1906.11241 (2019).

[28] K. Akiyama *et al.* (Event Horizon Telescope), *Astrophys. J. Lett.* **930**, L12 (2022).

[29] K. Akiyama *et al.* (Event Horizon Telescope), *Astrophys. J. Lett.* **930**, L13 (2022).

[30] C. Bambi, K. Freese, S. Vagnozzi, and L. Visinelli, *Phys. Rev. D* **100**, 044057 (2019).

[31] S. Vagnozzi and L. Visinelli, *Phys. Rev. D* **100**, 024020 (2019).

[32] R. Kumar and S. G. Ghosh, *The Astrophysical Journal* **892**, 78 (2020).

[33] P.-C. Li, M. Guo, and B. Chen, *Phys. Rev. D* **101**, 084041 (2020).

[34] M. Zhang and J. Jiang, *Phys. Rev. D* **103**, 025005 (2021).

[35] T. Bronzwaer and H. Falcke, *Astrophys. J.* **920**, 155 (2021), arXiv:2108.03966 [astro-ph.HE].

[36] B. P. Singh, *Annals of Physics* **441**, 168892 (2022).

[37] N. U. Molla and U. Debnath, *Annals of Physics* **453**, 169304 (2023).

[38] R. Roy, S. Vagnozzi, and L. Visinelli, *Phys. Rev. D* **105**, 083002 (2022).

[39] A. Anjum, M. Afrin, and S. G. Ghosh, *Physics of the Dark Universe* **40**, 101195 (2023).

[40] M. Afrin, R. Kumar, and S. G. Ghosh, *Monthly Notices of the Royal Astronomical Society* **504**, 5927–5940a (2021) arXiv:2102.10289 [gr-qc].

[41] B. Hamil and B. Lütfüoğlu, *Physics of the Dark Universe* **42**, 101293 (2023).

[42] V. Perlick and O. Y. Tsupko, *Physics Reports* **947**, 1–39 (2022).

[43] T. Mirzaev, S. Li, B. Narzilloev, I. Hussain, A. Abdujabbarov, and B. Ahmedov, *Eur. Phys. J. Plus* **138**, 47 (2023).

[44] B. Narzilloev, I. Hussain, A. Abdujabbarov, B. Ahmedov, and C. Bambi, *Eur. Phys. J. Plus* **136**, 1032 (2021), arXiv:2110.01772 [gr-qc].

[45] A. Al-Badawi, M. Alloqulov, S. Shaymatov, and B. Ahmedov, *Chin. Phys. C* **48**, 095105 (2024), arXiv:2401.04584 [gr-qc].

[46] A. K. Ror, R. Gupta, A. Aryan, S. B. Pandey, S. R. Oates, A. J. Castro-Tirado, and S. Kumar, *Astrophys. J.* **971**, 163 (2024), arXiv:2406.01220 [astro-ph.HE].

[47] A. Einstein, *Science* **84**, 506 (1936).

[48] P. Schneider, J. Ehlers, and E. E. Falco, *Gravitational Lenses* (1992).

[49] K. S. Virbhadra and G. F. R. Ellis, *Phys. Rev. D* **62**, 084003 (2000), arXiv:astro-ph/9904193.

[50] K. S. Virbhadra, D. Narasimha, and S. M. Chitre, *Astron. Astrophys.* **337**, 1 (1998), arXiv:astro-ph/9801174.

[51] K. S. Virbhadra, *Phys. Rev. D* **106**, 064038 (2022), arXiv:2204.01879 [gr-qc].

[52] K. S. Virbhadra, *Phys. Rev. D* **79**, 083004 (2009), arXiv:0810.2109 [gr-qc].

[53] K. S. Virbhadra, *Can. J. Phys.* **102**, 512 (2024), arXiv:2204.01792 [gr-qc].

[54] K. S. Virbhadra and C. R. Keeton, *Phys. Rev. D* **77**, 124014 (2008), arXiv:0710.2333 [gr-qc].

[55] C. G. Darwin, *Proceedings of the Royal Society of London. Series A. Mathematical and Physical Sciences* **249**, 180 (1959).

[56] V. Bozza, *Phys. Rev. D* **66**, 103001 (2002), arXiv:gr-qc/0208075.

[57] S. Frittelli, T. P. Kling, and E. T. Newman, *Phys. Rev. D* **61**, 064021 (2000), arXiv:gr-qc/0001037.

[58] E. F. Eiroa, G. E. Romero, and D. F. Torres, *Phys. Rev. D* **66**, 024010 (2002).

[59] V. Bozza, *Phys. Rev. D* **67**, 103006 (2003), arXiv:gr-qc/0210109.

[60] E. F. Eiroa and D. F. Torres, *Phys. Rev. D* **69**, 063004 (2004).

[61] R. Whisker, *Phys. Rev. D* **71**, 064004 (2005), arXiv:astro-ph/0411786.

[62] E. F. Eiroa and C. M. Sendra, *Phys. Rev. D* **86**, 083009 (2012), arXiv:1207.5502 [gr-qc].

[63] A. Bhadra, *Phys. Rev. D* **67**, 103009 (2003), arXiv:gr-qc/0306016.

[64] J. Kumar, S. U. Islam, and S. G. Ghosh, *Astrophys. J.* **938**, 104 (2022), arXiv:2209.04240 [gr-qc].

[65] J. Kumar, S. U. Islam, and S. G. Ghosh, *Eur. Phys. J. C* **82**, 443 (2022), arXiv:2109.04450 [gr-qc].

[66] S. U. Islam and S. G. Ghosh, *Phys. Rev. D* **103**, 124052 (2021), arXiv:2011.10208 [gr-qc].

[67] R. Kumar, S. U. Islam, and S. G. Ghosh, *Eur. Phys. J. C* **80**, 1128 (2020), arXiv:2004.12970 [gr-qc].

[68] S. U. Islam, R. Kumar, and S. G. Ghosh, *JCAP* **09**, 030 (2020), arXiv:2004.01038 [gr-qc].

[69] B. Narzilloev, S. Shaymatov, I. Hussain, A. Abdujabbarov, B. Ahmedov, and C. Bambi, *Eur. Phys. J. C* **81**, 849 (2021), arXiv:2109.02816 [gr-qc].

[70] S. U. Islam, S. G. Ghosh, and S. D. Maharaj, *Chin. J. Phys.* **89**, 1710 (2024), arXiv:2203.00957 [gr-qc].

[71] E. F. Eiroa and C. M. Sendra, *Class. Quant. Grav.* **28**, 085008 (2011), arXiv:1011.2455 [gr-qc].

[72] A. Övgün, *Phys. Rev. D* **99**, 104075 (2019), arXiv:1902.04411 [gr-qc].

[73] S. Panpanich, S. Ponglertsakul, and L. Tannukij, *Phys. Rev. D* **100**, 044031 (2019), arXiv:1904.02915 [gr-qc].

[74] K. A. Bronnikov and K. A. Baleevskikh, *Grav. Cosmol.* **25**, 44 (2019), arXiv:1812.05704 [gr-qc].

[75] N. U. Molla, S. G. Ghosh, and U. Debnath, *Phys. Dark Univ.* **44**, 101495 (2024).

[76] S. U. Islam, J. Kumar, and S. G. Ghosh, *JCAP* **10**, 013 (2021), arXiv:2104.00696 [gr-qc].

[77] R. Kumar, S. G. Ghosh, and A. Wang, *Phys. Rev. D* **101**, 104001 (2020), arXiv:2001.00460 [gr-qc].

[78] N. U. Molla and U. Debnath, *Int. J. Geom. Meth. Mod. Phys.* **19**, 2250183 (2022).

[79] N. U. Molla and U. Debnath, *Astrophys. J.* **947**, 14 (2023).

[80] N. U. Molla and U. Debnath, *Annals Phys.* **453**, 169304 (2023), arXiv:2212.02104 [gr-qc].

[81] P. V. P. Cunha and C. A. R. Herdeiro, *Gen. Rel. Grav.* **50**, 42 (2018), arXiv:1801.00860 [gr-qc].

[82] S. U. Islam and S. G. Ghosh, *Physical Review D* **103** (2021), 10.1103/physrevd.103.124052.

[83] S. Y. F. Liu and Y. Yin, *Phys. Rev. D* **104**, 054043 (2021).

[84] N. U. Molla and U. Debnath, *Int. J. Mod. Phys. A* **36**, 2150210 (2021).

[85] S.-W. Wei, Y.-X. Liu, C.-E. Fu, and K. Yang, *Journal of Cosmology and Astroparticle Physics* **2012**, 053 (2012).

[86] N. U. Molla, A. Ali, U. Debnath, and S. S. Gunasekaran, *Phys. Scripta* **99**, 075019 (2024).

[87] X. Pang and J. Jia, *Class. Quant. Grav.* **36**, 065012 (2019), arXiv:1806.04719 [gr-qc].

[88] P. Bessa, *Phys. Rev. D* **108**, 024062 (2023), arXiv:2304.08141 [gr-qc].

[89] S.-S. Zhao and Y. Xie, *JCAP* **07**, 007 (2016), arXiv:1603.00637 [gr-qc].

[90] C.-K. Qiao and M. Zhou, *JCAP* **12**, 005 (2023), arXiv:2212.13311 [gr-qc].

[91] F. Feleppa, V. Bozza, and O. Y. Tsupko, *Phys. Rev. D* **110**, 064031 (2024), arXiv:2406.07703 [gr-qc].

[92] R. Percacci, *An Introduction to Covariant Quantum Gravity and 100 Years of General Relativity*, Vol. 3 (World Scientific, 2017).

[93] B. Koch and F. Saueressig, *Classical and Quantum Gravity* **31**, 015006 (2013).

[94] A. Bonanno and M. Reuter, *Phys. Rev. D* **73**, 083005 (2006).

[95] J. N. Borissova and A. Platania, *Journal of High Energy Physics* **2023** (2023), 10.1007/jhep03(2023)086.

[96] D. Becker and M. Reuter, *Journal of High Energy Physics* **2012** (2012), 10.1007/jhep07(2012)086.

[97] K. FALLS, D. F. LITIM, and A. RAGHURAMAN, *International Journal of Modern Physics A* **27**, 1250019 (2012), <https://doi.org/10.1142/S0217751X12500194>.

[98] J. M. Pawłowski and D. Stock, *Physical Review D* **98** (2018), 10.1103/physrevd.98.106008.

[99] A. Platania, “Black holes in asymptotically safe gravity,” in *Handbook of Quantum Gravity* (Springer Nature Singapore, 2023) p. 1–65.

[100] A. Eichhorn and A. Held, “Black holes in asymptotically safe gravity and beyond,” (2022), arXiv:2212.09495 [gr-qc].

[101] J. M. Pawłowski and J. Tränkle, *Phys. Rev. D* **110**, 086011 (2024), arXiv:2309.17043 [hep-th].

[102] T. Denz, J. M. Pawłowski, and M. Reichert, *The European Physical Journal C* **78**, 1 (2018).

[103] B. Knorr and M. Schiffer, “Non-perturbative propagators in quantum gravity,” (2021), arXiv:2105.04566 [hep-th].

[104] B. Knorr, C. Ripken, and F. Saueressig, “Form factors in quantum gravity - contrasting non-local, ghost-free” (2021), arXiv:2111.12365 [hep-th].

[105] T. Draper, B. Knorr, C. Ripken, and F. Saueressig, *Physical Review Letters* **125** (2020), 10.1103/physrevlett.125.181301.

[106] A. Platania and J. Redondo-Yuste, “Diverging black hole entropy from quantum infrared non-localities” (2023), arXiv:2303.17621 [hep-th].

[107] B. Knorr, C. Ripken, and F. Saueressig, in *Handbook of Quantum Gravity* (Springer, 2024) pp. 1–49.

[108] V. Perlick and O. Y. Tsupko, *Phys. Rept.* **947**, 1 (2022), arXiv:2105.07101 [gr-qc].

[109] E. Ghorani, B. Pulić, F. Atamurotov, J. Rayimbaev, A. Abdubabarov, and D. Demir, *Eur. Phys. J. C* **83**, 318 (2023), [Erratum: Eur.Phys.J.C 83, 360 (2023)], arXiv:2304.03660 [gr-qc].

[110] S. Vagnozzi, R. Roy, Y.-D. Tsai, L. Visinelli, M. Afrin, A. Allahyari, P. Bambhaniya, D. Dey, S. G. Ghosh, P. S. Joshi, *et al.*, *Classical and Quantum Gravity* **40**, 165007 (2023).

[111] F. Atamurotov, I. Hussain, G. Mustafa, and A. Övgün, *Chinese Physics C* **47**, 025102 (2023).

[112] K. Akiyama, A. Alberdi, W. Alef, K. Asada, R. AZULY, *et al.*, *Astrophys. J. Lett* **875**, L1 (2019).

[113] D. Arora, N. U. Molla, H. Chaudhary, U. Debnath, F. Atamurotov, and G. Mustafa, *Asymptotic Phys. J. C* **83**, 995 (2023), arXiv:2308.13901 [gr-qc].

[114] C. Bambi, K. Freese, S. Vagnozzi, and L. Visinelli, *Phys. Rev. D* **100**, 044057 (2019), arXiv:1904.12983 [gr-qc].

[115] K. S. Virbhadra and G. F. R. Ellis, *Phys. Rev. D* **65**, 103004 (2002).

[116] C.-M. Claudel, K. S. Virbhadra, and G. F. R. Ellis, *J. Math. Phys.* **42**, 818 (2001).

[117] 086. L. Adler and K. S. Virbhadra, *Gen. Rel. Grav.* **54**, 93 (2022), arXiv:2205.04628 [gr-qc].

[118] 102. Tsukamoto, *Physical Review D* **95**, 064035 (2017).

[119] N. Tsukamoto, *Physical Review D* **94**, 124001 (2016).

[120] J. Chagoya, C. Ortiz, B. Rodríguez, and A. A. Roque, *Class. Quant. Grav.* **38**, 075026 (2021), arXiv:2007.09473 [gr-qc].

[121] V. Bozza, S. Capozziello, G. Iovane, and G. Scarpetta, *Gen. Rel. Grav.* **33**, 1535 (2001), arXiv:gr-qc/0102068.

[122] S. Gillessen, P. Plewa, F. Eisenhauer, R. Sari, I. Waisberg, M. Habibi, O. Pfuhl, E. George, J. Dexter, S. von Fellenberg, *et al.*, *The Astrophysical Journal* **837**, 30 (2017).

- [123] S. Liebes, Phys. Rev. **133**, B835 (1964).
- [124] Y. Mellier, Ann. Rev. Astron. Astrophys. **37**, 127 (1999).
- [125] M. Bartelmann and P. Schneider, Phys. Rept. **340**, 291 (2001).
- [126] F. Schmidt, Phys. Rev. D **78**, 043002 (2008).
- [127] J. Guzik, B. Jain, and M. Takada, Phys. Rev. D **81**, 023503 (2010).
- [128] V. Bozza and L. Mancini, [Gen. Rel. Grav. \*\*36\*\*, 435 \(2004\)](#), [arXiv:gr-qc/0305007](#).
- [129] J. Kormendy and L. C. Ho, [Ann. Rev. Astron. Astrophys. \*\*51\*\*, 511 \(2013\)](#), [arXiv:1304.7762 \[astro-ph.CO\]](#).